Genomic and Transcriptomic Landscapes of MEN1-Wild-Type Low-Grade Metastatic Pancreatic NETs Uncover Key Oncogenic Drivers and Targetable Pathways

Md Hafiz Uddin[1#], Zaid Mahdi[2#], Irfana Muqbil[3#], Brendon R. Herring[4#], Bart Rose[4], Husain Y. Khan[1], Yiwei Li[1], Amro Aboukameel[1], Sahar F. Bannoura[1], Hugo Jimenez[1], Allan Johansen[5], Mohammad Najeeb Al-Hallak[1], Ibrahim Azar[1,6], Amr Mohamed[7], Tarik Hadid[1], Nitin Vaishampayan[1], Yang Shi[1], Yin Wan[1], Vy Ong[1], Gregory Dyson[1], Rafic Beydoun[8], Miguel Tobon[1], Eliza W. Beal[1], Herbert Chen[4], Anthony F. Shields[1], Philip A. Philip[1,9], Jennifer Beebe-Dimmer[1], Ramzi M. Mohammad[1], Boris C. Pasche[1], Bassel F. El-Rayes[4*], Asfar S. Azmi[1]*

*Corresponding author

#authors contributed equally

Affiliations: [1]Karmanos Cancer Institute, Detroit, MI, [2]Emory Winship Cancer Institute, Atlanta, GA, [3]Lawrence Technological University, Southfield, MI, [4]O'Neal Comprehensive Cancer Center, University of Alabama at Birmingham, Birmingham, AL, [5]Department of Cancer Biology, Wake Forest University, Winston-Salem, NC, [6]Trinity Health Oakland, Pontiac , MI, [7]UH Seidman Cancer Center, University Hospitals, Case Western Reserve University, Cleveland, OH, [8]Department of Pathology, Wayne State University School of Medicine, Wayne State University, Detroit, MI [9]Henry Ford Health System, Detroit, MI.

***Address of Correspondence:**

Bassel F. El-Rayes, MD

Albert F. LoBuglio Endowed Chair for Translational Cancer Research

Division Director, Hematology and Oncology

Deputy Director, O'Neal Comprehensive Cancer Center

Heersink School of Medicine, UAB

Email: belrayes@uabmc.edu

Asfar S. Azmi, PhD.
Department of Oncology
Wayne State University School of Medicine
4100 John R, HWCRC 740.2
Karmanos Cancer Institute
Detroit, MI 48201
Tel: +1313 258 6148
Email: azmia@karmanos.org

Funding: Work in the lab of Asfar S. Azmi is supported by NIH 5R01CA240607. The authors thank the Karmanos Partners Fund for supporting this study.

Abstract

Sporadic pancreatic neuroendocrine tumors (pNETs) with wild type MEN1 represent a major yet largely ignored subset whose biology and metastatic potential remain poorly understood. Because metastasis can occur despite low histologic grade and modest mutational burden, we hypothesized that metastatic competence in MEN1-wild-type pNETs reflects quantitative reinforcement of shared oncogenic pathways rather than distinct mutational processes. We profiled 75 primary low-grade pNETs by whole-exome and RNA sequencing, including 25 percent with lymph node and/or liver metastasis, and integrated genomic and transcriptomic data to connect pathway lesions with expression state. Metastatic tumors showed a slight increase in mutation frequency but conserved base-substitution spectra relative to non-metastatic cases, and adverse clinicopathologic features were enriched in Grade 2 disease. Aggregating alterations to pathways revealed broad convergence on canonical networks, with transcriptomic analyses demonstrating cohort-wide enrichment of Calcium, WNT, and KRAS/PI3K-AKT programs in metastasis. Intersection of significantly mutated genes with differentially expressed genes identified a focused 29-gene overlap, including RYR1 and ZNF273, that marks these convergent axes and distinguishes metastatic from non-metastatic tumors. Gene set enrichment confirmed preferential activation of Calcium, WNT, and PI3K-AKT signaling in metastatic tumors, consistent with a network-intensity model of progression. Finally, upstream-regulator analysis (iPathwayGuide) and gene-centric perturbation mapping (Gene2Drug) nominated candidate targeted and repurposable agents predicted to reverse the metastatic expression phenotype and flagged drugs unlikely to provide benefit, yielding a prioritized, testable therapeutic shortlist which includes fasudil and spaglumic acid. Convergent, domain-specific mutational patterns in highly mutated genes such as ZNF273 and CLCA1 define a molecular signature that could stratify metastatic risk in low-grade pNETs. Collectively, our data reframe metastasis in MEN1-wild-type low-grade pNETs as a property of pathway state rather than mutation quantity and provide a translational blueprint for biomarker-guided therapy development focused on Calcium, WNT, and KRAS/PI3K hubs.

Keywords: Pancreatic neuroendocrine tumors, genomic and transcriptomic characterization, low grade, metastasis, mutation, therapeutic candidates.

Introduction

Neuroendocrine tumors (NETs) arise from the hormone-producing cells of various organs throughout the body and include pancreatic NETs (pNETs), medullary thyroid cancer, gastrointestinal (GI) NETs, bronchopulmonary NETs, and paraganglioma/pheochromocytoma[1]. Over 50% of patients with pancreatic NETs develop isolated hepatic metastases[1]. According to the American Cancer Society's estimate, in the United States over 4,000 individuals were diagnosed with pNETs in 2020 (ACS Statistics)[2]. Overall survival for pNETs can be relatively long compared to other cancers, leading to a higher number of cases of this disease at any given time[3,4]. Pancreatic neuroendocrine tumors (pNETs) are heterogeneous neoplasms with rising incidence and substantial clinical variability, ranging from indolent lesions to tumors that metastasize despite low histologic grade, thus the management of pNETs remains clinically challenging[2]. Improvements in the identification of actionable oncogenic drivers or systemic treatments for this growing patient population have been at best modest in recent decades. Therefore, pNETs remain a significant unmet clinical problem and in urgent need of newer biomarkers as well as more effective therapeutics.

pNETs can result from heritable genetic or somatic non-familial mutations[5,6]. Earlier, large scale genomic studies revealed that loss of Multiple Endocrine Neoplasia Type 1 (MEN1), Death-Domain-Associated protein (DAXX), and α Thalassemia/mental Retardation Syndrome X-linked (ATRX) genes as the major genetic aberrations in pNETs[7]. Additionally, the hyperactivation of PI3K-Akt-mTOR through loss of tumor suppressor PTEN has been well documented as a main driver in pNETs[8,9]. Molecular studies over the past decade have defined recurrent alterations in MEN1, DAXX, and ATRX, and frequent perturbations of PI3K-mTOR signaling, establishing a canonical framework for tumorigenesis and motivating targeted therapy trials[7,10-13]. These genomic advances translated into clinically meaningful gains with agents such as everolimus[14] and sunitinib, which prolong progression-free survival in advanced disease[12], yet durable control and robust biomarkers remain limited [11,15,16]. More recent multi-omic and population-level analyses underscore that tumor evolution and outcome are not fully explained by the presence or absence of MEN1/DAXX/ATRX lesions alone, and that broader network-level perturbations likely shape malignant potential and therapeutic response[17-19]. Within this landscape, MEN1-wild type disease

constitutes a major and under characterized subset of sporadic pNETs in which the determinants of metastatic behavior and drug sensitivity remain unclear.

Despite progress in cataloging mutations, key biological and clinical questions persist[20]. Much of the field's mechanistic understanding derives from cohorts enriched for MEN1-mutant tumors or from studies that emphasize single-gene drivers rather than pathway state, leaving MEN1-wild type pNETs relatively unresolved[18,21,22]. While PI3K-mTOR axis activity is common, it incompletely predicts metastatic risk or treatment benefit, implying that additional signaling circuits and microenvironmental interactions modulate aggressiveness[17,23]. The tumor mutational burden in pNETs is generally low to moderate and does not consistently stratify outcomes, raising the possibility that metastatic competence may arise from quantitative reinforcement of shared oncogenic pathways rather than qualitative shifts in mutational processes[24].

To address these gaps, we assembled and profiled a rigorously curated cohort of MEN1-wild type low-grade pNETs using matched whole-exome and RNA sequencing and integrated the resulting data to connect genomic lesions with transcriptional state. Our guiding hypothesis was that metastatic behavior in histologically low-grade tumors reflects convergence on a limited set of oncogenic pathways that are quantifiably more active in metastasis and that these pathway states can be mapped to pharmacologic space using complementary in silico approaches. We therefore contrasted non-metastatic and metastatic cases, aggregated mutations to pathway-level signatures, and asked which axes show concordant genomic/transcriptomic deregulation and cohort-wide enrichment by gene set analysis.

Our integrated analysis supports a revised view of aggressiveness in MEN1-wild type pNETs. We show that metastatic tumors exhibit only modest increases in mutation frequency relative to non-metastatic counterparts and conserve base-substitution spectra, yet display stronger engagement of convergent signaling programs, notably Calcium signaling, WNT, and KRAS/PI3K-related pathways, with a small set of genes showing overlap between somatic alteration and differential expression. Our framework integrates pathway-level mutation maps with transcriptomic enrichment and drug-prediction analyses to move beyond catalogs toward actionable network states. Current study provides a translational bridge by applying iPathwayGuide and Gene2Drug to nominate candidate therapeutics that are predicted to reverse

137 the metastatic expression phenotype and to identify agents unlikely to help in this context. The
138 methodology is supported by prior validations of these tools for mechanistic inference and drug
139 prioritization, and by reports implicating RYR1 dysregulation and related calcium handling
140 machinery in tumor biology across solid cancers[25-28]. Together, this study reframes metastatic
141 propensity as a property of network intensity and transcriptional reinforcement rather than new
142 mutational categories, and it outlines how integrated genomics and transcriptomics can prioritize
143 therapies for a clinically important yet understudied subset of pNETs.

144 **Methods**

145

146 **Collection, processing and sequencing of patient samples:**

147

148 Under an IRB approved protocol (STUDY00001739), a total of 104 Formalin-Fixed,
149 Paraffin-Embedded (FFPE) tissues (98 low grade pancreatic neuroendocrine tumor (pNET) and
150 six normal pancreatic) from the Emory University tissue biobank were sectioned and the genomic
151 DNA was extracted using QIAamp DNA FFPE Tissue Kit (Qiagen, Germany). Sex was considered
152 as a biological variable and average age of the patients was 55.83 years. Among the 98 pNET
153 tissues, eight samples did not have information related to grade and stage were therefore excluded.
154 Next, eight samples failed QC and were excluded. Finally, seven samples are not classified as
155 Grade 1 or 2 therefore excluded (Figure 1A shows tissue selection schema).

156

157 **Collection of pathological records:**

158

159 Primary tumor characteristics of the pNET patients were obtained from the histo- and
160 cytopathology registry at Emory University. Data collected included patient gender, WHO-defined
161 tumor differentiation grade (Grade 1 or Grade 2), proliferation index (Ki-67), and evidence of
162 invasion or metastasis. For each patient, information was extracted from the pathological reports
163 of the primary and/or metastatic lesions. When multiple reports were available, the record closest
164 in date but always preceding the biopsy was considered.

165

166 **Whole exome sequencing:**

For whole exome sequencing (WES), DNA samples from pNET and normal tissues were fragmented by using sonication and subjected to library construction in blinded fashion. Exome capture was performed using the SureSelect Human All Exon V6 Kit (Agilent Technologies) following the vendor's protocol. Sequencing was performed using the Illumina Hiseq X Ten with 150-bp paired-end reads for a total of 40 million reads. Prior to alignment, the low-quality reads were removed. Reads were aligned to the reference genome using Burrows-Wheeler Alignment (BWA). Picard tools were utilized to identify and remove duplicate reads from the BAM files generated by BMA. The resulting BAM files were indexed and sorted by samtools.

Mutational signature analysis:

The Genome Analysis Toolkit (GATK) was utilized to identify the genomic variants in the WES data. Somatic variant calls were generated with GATK Mutect2, which assigned an accurate confidence score to each putative mutation call and evaluated new potential variants. Biological functional annotations for the identified somatic variants were performed using Annovar. Somatic copy number variants (CNVs) were detected using Facets. The R Bioconductor package, Maftools were utilized for summarizing, analyzing and visualizing. Mutation Annotation Format (MAF) files generated from GATK, which created the oncoplots, transition and transversion plots, and lollipop mutation diagrams to visualize the somatic mutations in pNET patients.

RNA-sequencing:

Total RNA was extracted from pNET and normal tissues using the miRNeasy mini kit from Qiagen. The primary pNETs and pancreatic normal FFPE (Formalin-Fixed, Paraffin-Embedded) tissues were sectioned, and the total RNA was extracted following manufacturer’s instruction (Qiagen, Germany). Total RNA-sequencing was conducted by LC Sciences. For total RNA sequencing, RNA integrity was checked with Agilent Technologies 2100 Bioanalyzer to ensure RIN >7 cutoff value. All the samples passed the quality control except four pNET samples. Approximately 10 µg of total RNA was used to isolate poly(A) mRNA employing poly-T oligo–conjugated magnetic beads (Invitrogen). The captured poly(A)+ or poly(A)- RNA fractions were

198 fragmented into short fragments using divalent cations under elevated temperature. The resulting
199 RNA fragments were then reverse transcribed to generate complementary DNA (cDNA) libraries
200 according to the manufacturer's protocol (Illumina, San Diego, CA, USA). The sequence library
201 was prepared following Illumina's TruSeq-stranded-total-RNA-sample preparation protocol.
202 Quality control analysis and quantification of the sequencing library were performed using Agilent
203 Technologies 2100 Bioanalyzer High Sensitivity DNA Chip. Paired-end sequencing was
204 performed on Illumina's NovaSeq 6000 sequencing system for a total of 40 million reads per
205 sample. The reads in Fastq format were mapped to the human genome using HIAST2. Expression
206 levels of mRNAs were quantified using StringTie[29] based on fragments per kilobase of transcript
207 per million mapped reads (FPKM), and the expression of transcripts generated from the same gene
208 were aggregated to obtain the expression level of the gene. Differentially expressed genes were
209 determined using the R Bioconductor package, applying the thresholds of absolute values of log2
210 (fold change) > 1 and a false discovery rate (FDR) < 0.05 for statistical significance.
211
212 **Inventory of clinically actionable putative therapeutic targets against somatic alterations:**
213
214 We prioritized candidate therapies by integrating pathway-level upstream regulator
215 inference (iPathwayGuide, Advaita Bio; AKB v18.1, 2025 release) with gene-centric drug
216 perturbation profiling (Gene2Drug, accessed 2025) using the same tumor set. Differentially
217 expressed genes (DEGs) were derived from metastatic versus non-metastatic low-grade pNETs
218 with gene symbols harmonized to HGNC. In iPathwayGuide, DEGs were mapped onto the Advaita
219 Knowledge Base and analyzed via impact analysis, which combines (i) over-representation
220 statistics and (ii) perturbation of pathway topology to model directionality across signaling
221 cascades. In parallel, Gene2Drug queried the subset of "overlapped" genes (significantly mutated
222 and differentially expressed in the same tumors) plus pathway-adjacent DEGs against
223 LINCS/Connectivity-Map derived perturbational signatures across multiple annotation spaces
224 (cancer gene perturbations, Gene Ontology, transcription factor target sets etc). For each
225 compound, an enrichment score was computed over rank-ordered drug-response profiles.
226
227 **Statistical analysis:**

228 All analyses were performed on primary low-grade pNETs with matched WES and RNA-
229 seq. For RNA-Seq, differential expressed genes were assessed with the R Bioconductor package
230 edgeR with the thresholds of absolute value of log2 (fold change) > 1 and FDR < 0.05. For WES
231 data, tumor mutational burden (TMB) was computed as somatic single-nucleotide variants and
232 short indels per callable megabase in the exome; base-substitution spectra were summarized in the
233 six canonical SNV classes. Differential mutated genes between the pNET and normal samples
234 were identified using the Fisher's exact test with a p-value < 0.05 and the difference in mutation
235 frequencies between the two groups greater than 20%. The R Bioconductor package clusterProfiler
236 was used for functional enrichment analysis, where the over-representation tests were used for
237 KEGG (Kyoto Encyclopedia of Genes and Genomes) pathway and Gene Ontology (GO)
238 categories used and gene set enrichment analysis (GSEA) was performed for the Molecular
239 Signatures Database (MSigDB) Hallmark gene set collections. Significantly enriched pathways,
240 GOs and gene sets were identified using FDR< 0.05.

241

242 **Results**

243 **Clinicopathologic stratification of low-grade pNETs for integrated genomic and**
244 **transcriptomic analysis**

245 From the institutional cohort of low-grade pNETs, we identified 104 patients with available
246 FFPE biopsy material and subjected all corresponding specimens to whole-exome sequencing
247 (WES) and RNA sequencing (RNA-seq) (**Figure 1A**). Samples were sequentially filtered to ensure
248 clinicopathologic and molecular data quality. Twenty-three cases were removed because they
249 failed prespecified QC metrics for nucleic acid yield or sequencing performance, lacked reliable
250 information on grade and/or stage, or could not be unequivocally classified as WHO Grade 1 or
251 Grade 2. After these exclusions, low-grade pNETs with high-quality genomic and transcriptomic
252 data were retained for downstream analyses. Metastatic cases within this refined cohort are
253 highlighted in **Figure 1A** (light pink boxes).

254 To investigate molecular determinants of metastatic behavior, the primary tumors were
255 subsequently stratified into two major categories according to their metastatic outcome (**Figure**

256 **1B**) including low-grade non-metastatic and metastatic pNETs. Both groups underwent a unified
257 workflow, including DNA and RNA extraction from FFPE blocks, WES and RNA-seq, and
258 integrated genomic-transcriptomic analysis for candidate target identification. Among the primary
259 tumors, 7 Grade-1 and 12 Grade-2 pNETs were with metastatic status (**Figure 1A**), providing a
260 clinically annotated set of cases for comparative analyses with non-metastatic counterparts.

261 The demographic and pathological characteristics of the sequenced cohort are summarized
262 in **Figures 1C-1D** and **Table 1**. Age at diagnosis displayed a wide distribution in both sexes, with
263 overlapping ranges and comparable median ages for male and female patients (**Figure 1C**),
264 indicating that metastatic propensity in this cohort is not driven by major age or sex imbalances.
265 In contrast, adverse histopathologic features were enriched among Grade 2 tumors. Grade 2 tumors
266 exhibited substantially higher rates of lympho-vascular invasion (LVI), peri-neural invasion (PNI),
267 and metastasis (METs) compared to Grade 1 (30-37% positive vs. 17-21% in Grade 1; **Figure**
268 **1D**). Collectively, these data define a well-curated set of primary low-grade pNETs with linked
269 clinical, histologic, and multi-omic profiles, and underscore the association between metastatic
270 potential and genomic/transcriptomic characteristics.

271 **Comprehensive landscape of somatic mutations in low-grade pNETs reveals conserved**
272 **mutational signatures across metastatic states**
273

274 The global mutational landscape of primary low-grade pNETs was next examined by
275 ordering tumors according to metastatic outcome and histologic grade (**Figure 2**). Across the
276 sequenced tumors, the overall tumor mutational burden (TMB) in exons including upstream,
277 downstream and non-coding sequences was moderate, with most cases harboring relatively low
278 number of mutations per megabase (Mb). A small subset of outliers exhibiting markedly elevated
279 TMB (**Figure 2A**). A similar pattern was observed when analysis was restricted to coding regions,
280 where exonic TMB paralleled the distribution of overall TMB (**Figure 2C**). Hypermutated tumors
281 were observed in both metastatic and non-metastatic groups, however, average mutation per Mb
282 were slightly higher in pNETs with metastatic status.

283 Inspection of mutation annotations showed that the majority of variants resided in non-
284 coding regions, predominantly intronic and intergenic, whereas exonic variants accounted for a

moderate fraction of the total mutational burden (**Figure 2B**). Within coding regions, nonsynonymous single-nucleotide variants (SNVs) and frameshift or non-frameshift insertions/deletions represented the dominant functional classes (**Figure 2D**). Synonymous substitutions and start/stop-altering events were comparatively infrequent, and the relative proportions of these exonic functional classes were broadly similar across tumors. Analysis of base-substitution spectra revealed a characteristic pyrimidine mutation pattern dominated by C>T transitions, with additional contributions from T>C and C>A changes (**Figure 2E**). This six-class SNV profile was highly consistent across the cohort and did not show obvious qualitative shifts between metastatic and non-metastatic tumors, suggesting that the operative mutational processes are shared across clinical subgroups.

To relate these genomic features to clinicopathologic parameters, tumors were annotated for metastatic status, site of spread, grade, and Ki-67 index (**Figures 2F-2I**). As expected, metastatic cases clustered toward higher histologic grades and higher Ki-67 percentages, and most distant recurrences involved the lymph node, with a smaller subset showing liver or multi-organ dissemination. Collectively, these data indicate that while classical clinicopathologic markers (grade, Ki-67, and site of spread) stratify aggressive behavior, metastatic propensity in low-grade pNETs is not simply explained by gross differences in mutational load or base-substitution patterns, motivating deeper pathway-level analyses.

Recurrently mutated genes and canonical cancer drivers in non-metastatic and metastatic pNETs

To delineate gene-level differences between indolent and aggressive disease, we next mapped somatic alterations across all the primary pNETs using oncoprint representations of the top 50 recurrently mutated genes together with seven canonical cancer-driver genes (**Figure 3** and **Supplementary Figure 1**). All tumors (including 56 non-metastatic and 19 metastatic) harbored at least one coding alteration in this gene set (100% altered in each cohort), underscoring the pervasive yet heterogeneous nature of the mutational landscape. Samples are ordered from left to right based on decreasing TMB, with the stacked bars above each column illustrating that missense variants comprising the majority of mutations, followed by frameshift and nonsense events. The multi-hit alterations were found to be very common in highly mutated cases.

314 In non-metastatic pNETs, somatic alterations were broadly distributed across a large set of
315 genes, with frequent mutations in large structural or membrane-associated genes (e.g., MUC17,
316 TTN, AHNAK, MUC16, FLG, MUC4, FLG2, MUC12) and numerous zinc-finger transcription
317 factors (ZNF729, ZNF208, ZNF9, ZNF43, ZNF99, ZNF493, ZNF721 and ZNF845) among others
318 (**Figure 3A**). Many of these genes showed multi-hit patterns in a subset of tumors, suggesting
319 ongoing selective pressure or a mutational bias toward these loci. Canonical tumor suppressors
320 and signaling components such as DAXX, ATRX, PIK3CA, RICTOR, PTEN, TSC2, mTOR were
321 also recurrently altered, typically through missense, nonsense, or frameshift mutations, consistent
322 with disruption of chromatin remodeling and PI3K-mTOR pathway signaling in a substantial
323 fraction of non-metastatic tumors.

324 Metastatic pNETs displayed a qualitatively similar mutational repertoire (**Figure 3B**). The
325 same broad classes of genes dominated the top mutated list, including mucins (MUC17, MUC16,
326 MUC12), cytoskeletal or scaffolding genes (AHNAK, TTN), and multiple zinc-finger genes
327 (ZNF9, ZNF43, ZNF208, ZNF729, ZNF761, ZNF813, ZNF430). As in the non-metastatic group,
328 these loci frequently carried multi-hit events, particularly in tumors with the highest TMB.
329 Canonical drivers in chromatin remodeling and PI3K-mTOR signaling were again recurrently
330 mutated across metastatic samples, indicating that these pathways are commonly perturbed.
331 Comparison of the right-hand barplots, which summarize the number of tumors mutated in each
332 gene, revealed extensive overlap in the most frequently altered genes between non-metastatic and
333 metastatic cohorts, with modest shifts in rank order for metastasis-specific drivers. Overall, these
334 data show that both non-metastatic and metastatic low-grade pNETs share a complex but largely
335 conserved set of recurrent somatic alterations, centered on mucin/structural genes, zinc-finger
336 transcription factors.

337 To complement the oncoprints, we contrasted gene-level mutation prevalence between
338 metastatic and non-metastatic pNETs using a bubble scatterplot (**Figure 3C**). Most bubbles fall
339 near the red dashed diagonal, indicating broad parity in mutation prevalence across disease states.
340 Nevertheless, a subset of bubbles deviates above the diagonal consistent with genes showing
341 relatively higher mutation frequency in metastatic tumors. Such frequency-shift signals in **Figure**
342 **3C** point to a limited set of genes that may modulate metastatic propensity. The dispersion pattern,
343 together with the oncoprints, supports a largely conserved mutational backbone with selective

344 frequency shifts in a limited gene subset rather than wholesale rewiring of the gene-level
345 landscape. These observations suggest that additional layers such as transcriptional programs,
346 pathway activity are likely required to explain metastatic divergence.

347 **Convergent disruption of canonical oncogenic pathways and enriched proliferative**
348 **programs in metastatic pNETs**
349

350 We next examined how the somatic mutational landscape in pNETs converges on
351 established oncogenic signaling pathways (**Figure 4**). To assess such biological relevance of the
352 observed mutations, we performed pathway enrichment analysis using the Maftools mutation
353 annotation framework. This analysis revealed significant enrichment in several oncogenic and
354 developmental pathways, including RTK-RAS signaling, WNT/β-catenin, NOTCH, Hippo, cell
355 cycle regulation, TGF-β signaling, PI3K/mTOR, Myc, and p53 pathways (**Figure 4A-4B**).
356 Notably, the mutated genes in the RTK-RAS, WNT, NOTCH, and Hippo pathways were found to
357 be activated in pancreatic cancer tissues[30], suggesting that these alterations may contribute to
358 pNET tumorigenesis through shared oncogenic mechanisms. Thus pathway-level aggregation
359 revealed that virtually all tumors harbor alterations in one or more canonical cancer pathways.
360 Although a subset of the many genes annotated to each pathway were mutated, these alterations
361 collectively affected the pathway deregulation rather than single-gene lesions which could be a
362 defining feature of pNET genomics. Cell-cycle regulators, MYC-related signaling, TP53, TGF-β,
363 and NRF2 stress-response components were also recurrently affected, supporting broad
364 involvement of growth-control, differentiation, and stress-adaptation modules in pNETs.

365 At the gene level, binary mutation maps for RTK-RAS, NOTCH, WNT, and Hippo
366 signaling highlighted extensive inter-tumoral heterogeneity with clear evidence of pathway
367 convergence (**Figure 4B**). Within each pathway, somatic mutations were distributed across
368 multiple receptors, core signal transducers, and transcriptional effectors. Core canonical drivers
369 (highlighted in red) and essential, often druggable, signaling nodes (highlighted in blue) were
370 mutated in overlapping but non-identical subsets of tumors, indicating that distinct combinations
371 of lesions can perturb the same signaling axis. Hypermutated tumors frequently carried multiple
372 hits within a given pathway, whereas lower-burden tumors tended to harbor single-gene

373 alterations, suggesting quantitative differences in pathway disruption while maintaining qualitative
374 convergence on the same networks.

375 To relate these alterations to metastatic behavior, we compared the sets of mutated genes
376 between non-metastatic and metastatic pNETs. Of all genes mutated in at least one tumor, 65
377 (22.3%) were shared between the two groups, whereas 206 (70.5%) and 21 (7.2%) were uniquely
378 mutated in non-metastatic and metastatic tumors, respectively (**Figure 4C**). Thus, although the
379 majority of mutated genes are restricted to metastatic tumors, a distinct subset of genes is
380 preferentially altered in non-metastatic disease, superimposed on a common core of shared lesions.
381 Functional enrichment of genes mutated in metastatic versus non-metastatic tumors revealed
382 significant over-representation of multiple KEGG pathways such as Calcium, PI3K-Akt, WNT
383 etc. signaling pathways linked to growth signaling, cell-matrix interaction, and intracellular
384 communication (**Figure 4D**), as well as hallmark gene sets such as mitotic spindle, E2F targets,
385 KRAS signaling etc. associated with cell-cycle progression, MYC activity, DNA damage
386 responses, and stress-adaptation programs (**Figure 4E**). NOTCH and WNT signaling pathways
387 are also found to be enriched in grade 2 metastatic pNETs (**Supplementary Figure 2**). Together,
388 these data indicate that pNETs, and particularly hypermutated and metastatic tumors, display
389 substantial gene-level heterogeneity but converge on a limited number of canonical oncogenic
390 pathways and proliferative programs that may underlie metastatic competence and provide rational
391 targets for therapeutic intervention.

392 **Transcriptomic reprogramming and metastasis-associated gene expression programs in low-**
393 **grade pNETs**

394 We first compared the transcriptomes of low-grade pNETs with normal pancreas to define
395 tumor-specific gene expression programs (**Figure 5**). The volcano plot revealed a substantial
396 transcriptional rewiring, with 3,187 genes significantly upregulated and 1,363 genes significantly
397 downregulated in tumors relative to normal tissue (**Figure 5A**). Among the most strongly
398 downregulated genes were the immune and signaling regulators MKNK1-AS1, SOS2, CXCL10,
399 TRAT1, and TRBV17, whereas highly upregulated transcripts included SNTG1, RIMS2, GPC6,
400 AL355255, and PTPRT, highlighting coordinated suppression of selected inflammatory/signal-
401 transduction modules and induction of genes implicated in synaptic signaling, adhesion, and

402 receptor regulation. The differential expression pattern was consistent when compared between
403 non-metastatic and metastatic categories in Grade 1, Grade 2 or all pNETs (**Supplementary**
404 **Figure 3**).

405 Unsupervised hierarchical clustering of all differentially expressed genes (DEGs)
406 segregated tumors into distinct expression clusters (**Figure 5B**). Although clusters were not
407 perfectly concordant with any single clinicopathologic variable, the annotation tracks
408 demonstrated that metastatic status, WHO grade, and tumor size were not randomly distributed
409 across the dendrogram. Metastatic and WHO Grade 2 tumors, and those >2 cm, tended to
410 aggregate within expression subgroups. These findings suggest that discrete transcriptomic states
411 underlie a spectrum of biological behavior within histologically low-grade pNETs.

412 To explore functional consequences of these transcriptional changes, we performed KEGG
413 pathway and Gene Ontology enrichment analyses on DEGs between non-metastatic and metastatic
414 tumors (**Figure 5C**). The top enriched KEGG pathways and GO biological process, cellular
415 component, and molecular function terms converged on programs related to cell-cycle regulation,
416 DNA replication and repair, extracellular matrix organization, cell-cell/cell-matrix interaction, and
417 cytokine/immune signaling, indicating that metastatic tumors are preferentially enriched for
418 proliferative, matrix-remodeling, and microenvironment-interacting gene sets.

419 Gene-set enrichment using curated KEGG and hallmark signatures further highlighted
420 these differences (**Figure 5D-5E**). In metastatic versus non-metastatic tumors, significantly
421 enriched pathways showed higher fold-enrichment and larger contributing gene counts for multiple
422 proliferative, stress-response, and signaling programs, including PI3K-Akt, Calcium, MAPK,
423 WNT, RAS signaling pathways in KEGG (**Figure 5D**) and KRAS signaling, E2F targets, mitotic
424 spindle in hallmark gene sets are consistent with mutation associated modulations. Together, these
425 data demonstrate that, despite their low histologic grade, pNETs exhibit extensive transcriptional
426 reprogramming relative to normal pancreas, and that metastatic competence is associated with a
427 distinct enrichment of gene expression programs supporting proliferation, stress adaptation, and
428 tumor microenvironment crosstalk.

429 **Integrated genomic-transcriptomic analysis identifies Calcium, WNT, and KRAS/PI3K**
430 **signaling as convergent axes in low-grade pNETs**

431 To pinpoint alterations that are both genetically and transcriptionally encoded in the same
432 tumors, we integrated somatic mutation and RNA-seq data from the low-grade pNET cohort
433 (**Figure 6**). Intersection of significantly mutated genes with DEGs revealed a relatively small but
434 potentially high-value overlap. A total of 176 genes (3.4%) were exclusively mutated, 4,902 genes
435 (96.0%) were exclusively differentially expressed, and only 29 genes (0.6%) were both
436 significantly mutated and differentially expressed (**Figure 6A**). Thus, while pNETs display broad
437 transcriptional reprogramming, a restricted subset of genes shows concordant DNA- and RNA-
438 level deregulation. The lower panel of **Figure 6A** shows that these 29 overlapping genes are
439 mutated at variable frequencies across non-metastatic and metastatic tumors. Among the overlaps,
440 zinc finger protein 273 gene ZNF273, intracellular calcium release channel gene ryanodine
441 receptor 1 (RYR1) showed highest mutation prevalence in metastatic cases.

442 Pathway mapping of the overlapping gene set highlighted Calcium signaling, WNT
443 signaling, and KRAS/PI3K-related programs as major convergent nodes. In the Calcium signaling
444 pathway, multiple genes exhibited somatic mutations in both non-metastatic and metastatic
445 tumors, with some genes mutated more frequently in metastatic samples (**Figure 6B**, upper panel).
446 The accompanying heatmap (**Figure 6B**, lower panel) shows that many of these same genes are
447 also differentially expressed, with distinct expression patterns between metastatic and non-
448 metastatic tumors, supporting functional perturbation of calcium-dependent signaling in clinically
449 aggressive disease. Calcium signaling along with motor proteins also highlighted when non-
450 metastatic and metastatic pNETs of Grade 2 were compared (**Supplementary Figure 4**). A similar
451 pattern was observed for the WNT pathway, efferocytosis, inflammatory response and E2F targets
452 (**Figure 6C** and **Supplementary Figure 5**) genes carried recurrent mutations across the cohort,
453 and several showed consistent expression shifts between metastatic and non-metastatic tumors,
454 suggesting that these signaling dysregulation arises through a combination of genetic lesions and
455 transcriptional remodeling.

456 We next focused on the Hallmark KRAS signaling DN gene set, which encompasses
457 downstream targets suppressed upon oncogenic KRAS activation. Several components of this gene

458 set were mutated at appreciable frequencies in both metastatic and non-metastatic tumors (**Figure**
459 **6D**, upper panel), and the corresponding heatmap (**Figure 6D**, lower panel) demonstrated coherent
460 expression changes across the cohort. These data imply that KRAS-related signaling, although not
461 always driven by classic KRAS mutations, is modulated through alterations in its downstream
462 effector network.

463 To assess whether these pathways are coordinately enriched at the transcriptomic level in
464 metastatic disease, we performed gene set enrichment analysis (GSEA) comparing metastatic
465 versus non-metastatic tumors. Calcium signaling, WNT signaling, and PI3K-AKT signaling were
466 all positively enriched in metastatic pNETs (**Figure 6E-6G**), with normalized enrichment scores
467 (NES) above 1, indicating a consistent, cohort-wide shift toward higher pathway activity in
468 metastatic pNETs. Collectively, these integrative analyses demonstrate that only a small fraction
469 of genes are both mutated and differentially expressed, but those that tend to cluster within a
470 limited set of signaling pathways most notably Calcium, WNT, and KRAS/PI3K-AKT that are
471 transcriptionally upregulated in metastatic tumors. These convergent axes likely represent key
472 molecular circuits underpinning metastatic competence in low-grade pNETs and may provide
473 rational targets for therapeutic intervention or biomarker development.

474 We have analyzed mutational patterns for top overlapping genes including ZNF273,
475 CLCA1, RYR1, CEACAM5, MYO3B and observed distinct distribution of mutations both in
476 percentage and types between non-metastatic and metastatic pNET samples (**Figure 6H-6I** and
477 **Supplementary Figure 6**). Lollipop plots of ZNF273 (NM_021148) in pNETs reveal a marked
478 increase in somatic alterations in metastatic versus non-metastatic tumors. In non-metastatic cases
479 (n = 56), ZNF273 is mutated in 17.9% of tumors, primarily through missense substitutions and a
480 smaller number of in-frame insertions and deletions distributed across the C-terminal zinc-finger
481 region (zf-H2C2_2) and, less frequently, the N-terminal KRAB_A-box domain. In contrast,
482 metastatic primaries (n = 19) show a substantially higher somatic mutation rate of 52.6%, with
483 multiple recurrent missense variants and additional frame-shift insertions affecting both the
484 KRAB_A-box and zinc-finger domains, indicating more disruptive lesions in the transcriptional
485 regulatory architecture of ZNF273. Collectively, these data demonstrate that metastatic pNETs are
486 enriched for structurally diverse and potentially more deleterious ZNF273 mutations compared

487 with non-metastatic tumors, consistent with a role for ZNF273 dysregulation in metastatic
488 competence.

489 **In-silico drug prioritization reveals candidate targeted and repurposable therapies for**
490 **metastatic low-grade pNETs**

491 To explore whether the molecular alterations identified in metastatic low-grade pNETs
492 might be pharmacologically tractable, we applied complementary pathway- and gene-centric drug
493 prediction strategies (**Figure 7**). Upstream regulator analysis using iPathwayGuide, which
494 integrates the direction and magnitude of DEGs with a curated drug-target interaction network,
495 nominated several compounds whose known targets were consistently perturbed in metastatic
496 versus non-metastatic tumors (**Figure 7A**). These agents showed large numbers of "consistent
497 DEGs" (bars to the right), indicating that the observed transcriptional changes in metastatic pNETs
498 would be expected to be reversed or attenuated by drug exposure, and therefore may represent
499 clinically actionable candidates in this setting. In contrast, a second group of drugs was predicted
500 to lack actionable changes or to drive gene-expression shifts discordant with those observed in
501 metastatic tumors based on similarly structured analyses (**Figure 7B**). These compounds, which
502 also showed substantial DEG coverage, may be less likely to provide benefit in metastatic low-
503 grade pNETs and could even be counter-therapeutic.

504 We next used Gene2Drug software to focus on specific genes that were both recurrently
505 altered and associated with high TMB in metastatic tumors following integration of exome and
506 RNA-seq data. This analysis highlighted ZNF273 and RYR1 as representative "overlapped" genes
507 whose perturbation may be central to the metastatic phenotype. Gene2Drug queried multiple
508 functional databases, including cancer drug perturbation signatures (CGP) and Gene Ontology
509 categories (BP, CC, MF) as well as transcription-factor-target (TFT) sets, to identify drugs that
510 reproducibly downregulate expression programs centered on these genes. For ZNF273, numerous
511 compounds demonstrated strong inhibitory (DOWN) signatures with relatively high enrichment
512 scores (ES; 0.65-0.75), suggesting that their transcriptional footprints oppose the ZNF273-
513 associated expression pattern in metastatic tumors (**Figure 7C** and **Supplementary Figure 7**). A
514 similar analysis for RYR1 yielded a partially overlapping but distinct set of candidate drugs (ES;
515 ~0.7) drawn from multiple annotation databases (**Figure 7D** and **Supplementary Figure 8**).

516 Although exploratory and requiring functional validation, these integrative analyses
517 demonstrate that metastatic low-grade pNETs harbor molecular alterations that map onto existing
518 pharmacologic space. By combining pathway-level upstream regulator analysis with gene-centric
519 perturbation signatures, our data nominates a focused set of candidates targeted and repurposable
520 agents that may be capable of modulating key transcriptional programs driven by ZNF273, RYR1,
521 and related networks in metastatic low-grade pNETs.

522

523 **Discussion**

524 Pancreatic neuroendocrine tumors lacking MEN1 mutations comprise a major and under
525 characterized subset. By profiling low-grade primary pNETs with whole-exome and RNA
526 sequencing, including 25 percent with documented metastasis, we close a key gap by showing that
527 metastatic behavior emerges from pathway-level convergence rather than general changes in
528 mutational burden. To our knowledge, this is the first comprehensive study integrating genomic
529 and transcriptomic landscapes of low-grade pNETs to distinguish metastatic from non-metastatic
530 disease. The central advance is that metastatic propensity in these histologically low-grade tumors
531 is not explained by bulk mutational load or shifts in substitution spectra but is constrained by
532 coordinated activation of Calcium, WNT, and KRAS/PI3K pathway programs. These are
533 detectable at the transcriptome level and overlap with a small set of genes that are both mutated
534 and differentially expressed, including ZNF273 and RYR1. Importantly, upstream regulator and
535 gene-centric perturbation analyses nominate tractable candidates predicted to reverse metastatic
536 expression states while flagging agents unlikely to benefit this population, providing a prioritized
537 therapeutic hypothesis for prospective validation. Our data suggest that convergent, domain-
538 specific mutational patterns in frequently mutated genes may constitute a molecular signature
539 capable of stratifying metastatic risk in low-grade pNETs. These findings refine a MEN1 centric
540 model of pNET tumorigenesis by shifting emphasis toward transcriptomic reinforcement of shared
541 oncogenic pathways rather than acquisition of unique mutational processes.

542 While Chan et al. (2018) and other research groups characterized molecular subtypes
543 defined by MEN1, DAXX, and ATRX mutations, their analyses primarily focused on MEN1-
544 mutant tumors, leaving the MEN1-wild type subset (which accounts for ~60% of pNETs) less

545 explored[17,18,23]. Our data position MEN1-wild type low-grade pNETs as tumors in which
546 metastatic potential arises from quantitative reinforcement of shared oncogenic circuits rather than
547 acquisition of new mutational processes. Clinicopathologic enrichment of adverse features in
548 Grade 2 tumors (**Figure 1D**) and a modest rise in mutation burden in metastatic cases (**Figure 2A**,
549 **2C**) occur without broad changes in base-substitution spectra (**Figure 2E**), indicating conserved
550 mutational mechanisms across disease states. Oncoprint analysis shows substantial overlap in
551 recurrently altered genes between non-metastatic and metastatic tumors, particularly involving
552 chromatin remodelers and PI3K-mTOR components (**Figure 3A-B**), while frequency skews for a
553 limited subset of genes are evident in metastasis (**Figure 3C**). This pattern reinforces the concept
554 that pathway activation, rather than mutational quantity, drives metastatic progression. These
555 findings refine earlier genomic observations showing that sporadic pNETs generally harbor low
556 to moderate TMB and recurrent mutations in chromatin-remodeling and PI3K-mTOR
557 pathways[31,32]. Moreover, recent reviews emphasize that PI3K/AKT/mTOR signaling alone does
558 not fully predict metastatic behavior, suggesting the involvement of broader network
559 reinforcement[33].

560 Virtually all tumors in our MEN1-wild-type, low-grade pNET cohort, carry alterations in
561 one or more hallmark pathways with convergence on RTK-RAS, WNT, NOTCH, Hippo, PI3K-
562 mTOR, MYC, TP53, TGF-β and NRF2 modules (**Figure 4A-4B**), while only a small fraction of
563 genes are uniquely mutated in metastases yet those genes collectively enrich growth and
564 communication pathways, including PI3K-Akt, WNT and Calcium signaling (**Figure 4C-4D**).
565 Differential expressions relative to normal pancreas show broad rewiring with 3,187 upregulated
566 and 1,363 downregulated genes (**Figure 5A**), and unsupervised clustering links specific
567 transcriptomic states to metastatic status, grade and size (**Figure 5B**). Metastases preferentially
568 activate E2F targets, mitotic spindles and KRAS-linked signatures together with matrix-interaction
569 programs (**Figure 5C-5E**). These data align with studies establishing convergent pathway biology
570 in pNETs in which diverse lesions perturb shared axes such as MEN1/DAXX/ATRX and PI3K-
571 mTOR, and extend them by showing that, in MEN1-wild-type disease, metastatic behavior tracks
572 with pathway intensity rather than the appearance of new categories of mutation[7,9]. The
573 transcriptional enrichment of PI3K-mTOR and KRAS-proximal programs in metastases is
574 concordant with the clinical activity of pathway-directed agents such as everolimus and sunitinib

575 in advanced pNETs, supporting a rationale for biomarker-guided intensification or combination
576 strategies in this subgroup[24,34].
577
578 Integrating mutations and RNA profiles from the same MEN1-wild-type low-grade
579 pNETs, we find that only a narrow fraction of genes shows concordant DNA/RNA deregulation
580 (29 of 5,107; 0.6%), yet these concentrate within three reproducible signaling axes including
581 Calcium, WNT, and KRAS/PI3K that are preferentially engaged in metastatic tumors (**Figure 6A-**
582 **6G**). In Calcium signaling, metastatic cases carry higher mutation frequencies and coherent
583 expression shifts across ryanodine-receptor and channel components (e.g., RYR1) with positive
584 pathway enrichment by GSEA (**Figure 6B, 6E**), nominating calcium-dependent excitability as a
585 metastasis-linked property in neuroendocrine epithelium. This aligns with broader evidence that
586 Ca2+ circuit remodeling supports invasion and survival across cancers while extending such
587 observations to pNETs[35-37]. In parallel, WNT nodes show recurrent lesions with consistent
588 transcriptional upregulation in metastasis (**Figure 6C, 6F**), resonating with reports that WNT/β-
589 catenin contributes to neuroendocrine tumor growth and invasiveness and is variably active in
590 pNENs[38,39]. Finally, although canonical KRAS mutations are uncommon in pNETs relative to
591 pancreatic ductal adenocarcinoma (PDAC), our data indicate modulation of the Hallmark KRAS-
592 signaling-DN program together with PI3K-AKT enrichment (**Figure 6D, 6G**), consistent with the
593 long-standing view from genomics that pNETs frequently perturb MEN1/DAXX/ATRX and
594 mTOR-PI3K pathways rather than RAS itself[7]. Clinically, this convergence provides a mechanistic
595 rationale for the efficacy of pathway-directed agents everolimus and sunitinib improved
596 progression-free survival in randomized trials and suggests combination strategies that co-target
597 PI3K/mTOR with WNT or Ca2+ effectors could be prospectively prioritized in metastatic, MEN1-
598 wild type disease[14,15]. Together, these findings argue that metastatic competence in low-grade
599 pNETs reflects quantitative reinforcement of a shared circuitry rather than wholesale pathway
600 rewiring, and they identify calcium, WNT, and KRAS/PI3K signaling as tractable hubs for
601 biomarker development and therapeutic testing (**Figure 6A-6G**).

602 Our findings identify ZNF273 and ZNF184 as a previously unappreciated Krüppel-
603 associated box (KRAB)-zinc finger axis linked to metastatic competence and poor outcome in
604 pNETs, extending prior genomic studies that emphasized MEN1, DAXX, ATRX and mTOR

605 pathway alterations but did not highlight KRAB-ZNFs as recurrent lesions[7,9,40,41]. Lollipop plots
606 show that ZNF273 is mutated in more than half of metastatic versus fewer than one fifth of non-
607 metastatic pNETs with metastatic cases exhibiting more disruptive missense and frameshift
608 variants across both the KRAB_A box and C2H2 zinc-finger domains (**Figure 6H-6I**). These
609 patterns align with pan-cancer observations that mutations targeting structurally critical zinc-finger
610 residues can rewire transcriptional programs that promote progression[42] and with growing
611 evidence that KRAB-ZNFs function as context-dependent oncogenic regulators[43,44]. Our results
612 indicate that KRAB-ZNFs may stratify metastatic risk within the otherwise genetically quiet pNET
613 landscape and warrant functional investigation as contributors rather than incidental passengers in
614 metastatic progression.

615

616 In this study, we used complementary pathway-level and gene-centric perturbation
617 analyses to nominate actionable and repurposable drugs and, equally important, to flag agents
618 predicted to be non-beneficial in metastatic disease (**Figure 7A-7D**). These results extend prior
619 genomic characterizations that emphasized MEN1/DAXX/ATRX and PI3K-mTOR lesions in
620 pNETs by mapping metastasis-linked transcriptional programs onto pharmacologic space rather
621 than solely onto mutation catalogs[7,9,18]. Upstream-regulator inference with iPathwayGuide aligned
622 large fractions of metastatic DEGs with drug targets, prioritizing compounds whose predicted
623 effects would counter the observed expression shifts (**Figure 7A**) while identifying others that
624 were discordant and therefore less likely to help (**Figure 7B**). This approach is methodologically
625 supported by prior descriptions of iPathwayGuide for mechanistic pathway and regulator
626 discovery[25]. Orthogonally, Gene2Drug queries centered on overlapped, metastasis-associated
627 genes highlighted ZNF273 and RYR1, each linked to reproducible DOWN signatures across
628 multiple knowledge bases with moderate to strong enrichment (ES, 0.65-0.75; **Figure 7C-7D**),
629 consistent with Gene2Drug's validated strategy of ranking drugs by their ability to reverse target-
630 pathway transcriptional activity[26]. While ZNF273 is novel in pNETs, RYR1 dysregulation has
631 been implicated in tumor progression and drug repositioning in other solid tumors and has
632 recurrent alterations reported in neuroendocrine contexts, supporting plausibility for functional
633 relevance in pNET biology[27,28]. Notably, our drug-prediction framework complements emerging
634 clinical sequencing data showing pathway perturbations in metastatic low-grade pNETs and

provides testable hypotheses to rationalize sensitivity and resistance, including the a priori identification of agents unlikely to benefit this subset[45]. Collectively, these data argue that metastasis in MEN1-wild type low-grade pNETs is accompanied by coherent, drug-modifiable transcriptional circuits with attention to the mixed evidence base surrounding pNET molecular subtypes and outcomes[9,18].

By deeply characterizing MEN1-wild-type, low-grade pNETs, we show that metastasis is a property of pathway state rather than simple mutation burden. Metastatic tumors exhibit slightly higher mutation frequencies but stronger activation of Calcium, WNT, and KRAS/PI3K signaling, converging on a 29-gene set that links genomic alterations to transcriptomic remodeling. Convergent activation of such programs distinguishes metastatic from non- metastatic tumors and connects directly to rational therapeutic choices. This framework shifts emphasis from single-gene events toward network activity and provides a blueprint for biomarker-guided combination trials in a clinically important subset of pNETs.

Acknowledgements

The authors acknowledge the contribution of Dr. Julie Boerner at the Karmanos Cancer Institute Biobanking and Histopathology Core for providing the tissue samples. The authors also acknowledge Brian Burns at the Tissue Procurement Lab Coordinator Winship Cancer Institute Cancer Tissue and Pathology Shared Resource. The authors acknowledge 2P30CA022453-39 Karmanos Cancer Institute, Cancer Center Support Grant. Funding from SKY Foundation Inc., Partners Funds and U Can-Cer Vive to Dr. Azmi is acknowledged.

Author contributions

ASA, BFE designed the study, wrote and revised the manuscript. MHU, ZM, IM, BRH, analyzed the data, wrote and revised the manuscript. YL, YS, YW, VO, GD, guided the statistical analyses. BR, HYK, AA, SFB, HJ, AJ, MNA, IA, AM, TH, NV, RB, MT, EWB, HC, AFS, PAP, JB, RMM, BCP edited and revised the manuscript.

Data availability statement

The genetic variant data from WES of the pNET tissue samples are available from EBI's (European Bioinformatics Institute) BioStudies repository under accession number S-BSST1766 (URL: https://www.ebi.ac.uk/biostudies/studies/S-BSST1766?key=0a84424e-187f-4c36-bc01-2d59ca9669b1). The RNA-Seq data from the FFPE and fresh pNET and adjacent normal tissues are available from EBI's ArrayExpress repository under accession number E-MTAB-14709 (URL: https://www.ebi.ac.uk/biostudies/arrayexpress/studies/E-MTAB-14709?key=3a110a96-fca4-438e-822f-5afe8aab97ca). All data generated or analyzed during this study will be made available along with code information on reasonable request for academic use.

Ethics approval and consent to participate

The study was approved by the Institutional Review Board (IRB) of Emory University (Atlanta, GA) with the IRB number of STUDY00001739 and of Karmanos Cancer Institute (Detroit, MI) with the IRB number of 034916MP2X. Each patient provided informed consent before participating in the study. The study protocol was approved by the Ethics Committee of Emory University (FWA00005792) and Karmanos Cancer Institute Wayne State University (FWA00002460).

Competing Interest declaration

There is no direct Conflict of Interest (COI) to declare. Unrelated COI is as follows: ASA is council member for Gerson Lehrman Group, Guidepoint. ASA received funding from Colorado Chromatography, Blackstone, Purple Biotec, and FanWave Therapeutics. BFE reports relationships with Seattle Genetics and in the advisory board of Exelixis, Beigene, and AstraZeneca. BFE received funding from Bristol-Myers Squibb, Merck, Astra Zeneca, and Boehringer Ingelheim. BCP reports on a relationship with TheraBionic Inc, and TheraBionic GmbH that includes equity or stocks. BCP received funding from Merck & Co Inc., Roche, Novartis, AstraZeneca, and Bristol Myers Squibb Co. PAP receive Honoraria: Bayer, Ipsen, Incyte,

696 Taiho Pharmaceutical, Astellas Pharma, BioNTech SE, Novocure, TriSalus Life Sciences,
697 SERVIER, Seagen. Consulting or Advisory Role: Celgene, Ipsen, Merck, TriSalus Life Sciences,
698 Daiichi Sankyo, SynCoreBio, Taiho Pharmaceutical Speakers' Bureau: Incyte Research Funding:
699 Bayer (Inst), Incyte (Inst), Merck (Inst), Taiho Pharmaceutical (Inst), Novartis (Inst), Regeneron
700 (Inst), Genentech (Inst), Halozyme (Inst), Lilly (Inst), Taiho Pharmaceutical (Inst), merus (Inst),
701 BioNTech SE (Inst) Uncompensated Relationships: Rafael Pharmaceuticals, Caris MPI Bassel El-
702 Rayes Consulting or Advisory Role: Pfizer Research Funding: Taiho Pharmaceutical (Inst), Bristol
703 Myers Squibb (Inst), Boston Biomedical (Inst), Novartis (Inst), Hoosier Cancer Research Network
704 (Inst), Five Prime Therapeutics (Inst), Merck (Inst), ICON Clinical Research (Inst),
705 AstraZeneca/MedImmune (Inst), Xencor (Inst), Merck (Inst), Bayer (Inst), MedImmune (Inst),
706 Adaptimmune (Inst), Pfizer (Inst), Novartis (Inst), IQVIA (Inst), Zymeworks (Inst), Covance (Inst),
707 Wayne State University (Inst), Boehringer Ingelheim (Inst) Emil Lou Stock and Other Ownership
708 Interests: Ryght Honoraria: Novocure, GlaxoSmithKline, Boston Scientific, Daiichi Sankyo/UCB
709 Japan (Inst) Consulting or Advisory Role: Novocure, Boston Scientific Research Funding:
710 Novocure, Intima Travel, Accommodations, Expenses: GlaxoSmithKline Uncompensated
711 Relationships: Minnetronix Medical, NomoCan, Caris Life Sciences Alex Patrick Farrell
712 Employment: Caris Life Sciences Stock and Other Ownership Interests: Caris Life Sciences
713 Jeffrey Swensen Employment: Caris Life Sciences Travel, Accommodations, Expenses: Caris Life
714 Sciences Matthew James Oberley Employment: Caris Life Sciences Leadership: Caris Life
715 Sciences Stock and Other Ownership Interests: Caris Life Sciences Travel, Accommodations,
716 Expenses: Caris Life Sciences Chadi Nabhan Employment: Ryght Leadership: Ryght Stock and
717 Other Ownership Interests: Ryght Sanjay Goel Stock and Other Ownership Interests: Johnson and
718 Johnson, Merck, Moderna Therapeutics Honoraria: GlaxoSmithKline Research Funding:
719 Dragonfly Therapeutics (Inst), Deciphera (Inst), Amgen (Inst), Genentech (Inst), Xilio
720 Therapeutics (Inst), Exelixis (Inst) Patents, Royalties, Other Intellectual Property: I have a patent
721 with a coinventor, John Mariadason, Ph.D, titled "Method Of Determining The Sensitivity Of
722 Cancer Cells To EGFR Inhibitors Including Cetuximab, Panitumumab And Erlotinib.," Patent No.
723 20090258364. AFS report relationships with Caris Life Sciences and in the safety committee of
724 Cogent Biosciences. AFS received funding from Taiho Pharmaceutical, Bayer, Boehringer
725 Ingelheim, Plexxikon, Eisai, Inovio Pharmaceuticals, H3 Biomedicine, Caris Life Sciences,
726 ImaginAb, Exelixis, Xencor, Lexicon, Daiichi Sankyo, Halozyme, Incyte, LSK BioPharma,

727 Esperas Pharma, Nouscom, Boston Biomedical, Astellas Pharma, AstraZeneca, Five Prime
728 Therapeutics, MSK Pharma, Alkermes, Repertoire Immune Medicines, Telix Pharmaceuticals,
729 Hutchison China Meditech, Seagen, Jiangsu Alphamab Biopharmaceuticals, Shanghai HaiHe
730 Pharmaceutical, TopAlliance BioSciences Inc (Inst), Gritstone Bio (Inst), SQZ Biotechnology
731 (Inst), Nuvation Bio (Inst), Sorrento Therapeutics (Inst), Torque (Inst), Abbisko Therapeutics
732 (Inst), IconOVir Bio (Inst), Amal Therapeutics (Inst), TheraBionic (Inst) Travel, Accommodations,
733 Expenses: GE Healthcare, Caris Life Sciences, TransTarget, ImaginAb, INOVIO Pharmaceuticals.
734 MNA reports as speaker for Ipsen, AstraZeneca, Guardant Health, Pfizer, and Takeda. Ibrahim
735 Azar receives Honoraria: MJH Life Sciences; Consulting or Advisory Role: AstraZeneca, Genmab
736 Nishant Gandhi; Employment: Caris Life Sciences. MHU, ZM, IM, BRH, BR, HYK, YL, AA,
737 SFB, HJ, AJ, IA, AM, TH, NV, YS, YW, VO, GD, RB, MT, EWB, HC, JB, RMM declares no
738 competing interests.
739
740
741
742
743
744
745
746
747
748
749
750
751
752

753 **Legends to Figures**

754 **Figure 1. Overview of patient inclusion and subclassification FFPE tissues. A.** Flowchart of
755 patient inclusion. From low grade pNETs patient cohort, FFPE biopsy tissues from 104 distinct
756 patients were selected. Total pool of samples was subject to whole exome sequencing (WES) and
757 RNA sequencing (RNA-seq). The filtering criteria that led to sample exclusion are highlighted in
758 light green. The final set of selected samples is depicted in white boxes. Metastatic samples are
759 highlighted in light pink. **B.** Subclassification of pNETs patients and samples processing schema.
760 The 75 primary pNETs were subclassified into two major categories based on their metastatic
761 outcome. **C.** Age distribution stratified by gender of the pNET cohort. The variable's distribution
762 and median were visualized with data points clustered on the boxplot. **D.** Percentage of lympho-
763 vascular invasion (LVI), peri-neural invasion (PNI) and metastasis (METs) in Grade 1 and Grade
764 2 pNET patients. Exact percentage shown on top of each bar. N, negative (blue); P, positive (red).
765 Credit: **Figure 1B** was Created with BioRender (https://biorender.com/).

766

767 **Figure 2. Landscape of large-scale genomic alterations detected in pNETs, ordered by**
768 **metastatic potential and differentiation grade. A.** Overview of genomic characteristics of
769 pNETs, tumor mutational burden (TMB) ordered by metastatic potential and differentiation
770 grade.For each pNET (n = 75), a number of genomic mutations per megabase (Mb) is shown. B.
771 Percentage of mutations for all mutation types in all pNET samples. **C.** Overview of exonic TMB
772 ordered by metastatic potential and differentiation grade. For each pNET (n = 75), a number of
773 exonic Mb is shown. **D.** Percentage of exonic mutations for all mutation types in all pNET samples.
774 **E.** Relative frequency (percentage) of pyrimidine point mutation as the total single nucleotide
775 variants (SNVs) with six categories for all pNET samples. **F.** Categorization of primary tumors
776 based on the patient's metastatic status. Metastatic patient samples are depicted in red and non-
777 metastatic patient samples are depicted in blue. **G.** Categorization of metastasis based on their sites.
778 Liver metastasis depicted in green, lymph node metastasis depicted in orange, metastasis in
779 multiple sites depicted in light purple and non-metastatic samples marked in blue. **H.**
780 Differentiation grade of the pNETs; grade 1 (G1) samples are shown in red and grade 1 (G1)
781 samples are shown in blue. **I.** Proliferation index (Ki-67) from the pathological record where scores

range 0-16 are represented as a gradient between dark purple as the lowest score to yellow as the highest score.

Figure 3. Landscape of somatic alterations and tumor mutational burden in the pNET study cohort. A. Oncoprint showing the top fifty recurrently mutated genes and seven canonical genes across 56 primary pNETs from the patients with non-metastatic status. **B.** Oncoprint showing the top fifty recurrently mutated genes and seven canonical genes across 19 primary pNETs from the patients with metastatic status. Each column represents an individual tumor, and each row represents a gene, ordered by decreasing mutation frequency. The stacked bar plot above the heatmap depicts tumor mutational burden (TMB; mutations per megabase) for each sample. The height of the bar reflects total TMB and the colors indicate the contribution of different mutation classes. The horizontal bar plot on the right shows the number of tumors harboring at least one mutation in each gene. Genes in the lower "Canonical" panel highlight established cancer-driver genes analyzed in this cohort. Colored boxes within the heatmap denote the mutation type observed in that gene-tumor pair: missense mutation (green), non-sense mutation (red), nonstop mutation (light pink), in-frame deletion (dark orange), in-frame insertion (beige), frameshift deletion (blue), frameshift insertion (purple), and multi-hit events (black; ≥2 mutations in the same gene in a given tumor). Grey cells indicate that no coding mutation was detected in that gene in the corresponding tumor. All variants shown are somatic single-nucleotide variants or small insertions/deletions that passed standard quality-control filters, and samples are ordered from left to right by decreasing TMB. **C.** Bubble scatterplot contrasting the prevalence of recurrent gene mutations in metastatic versus non-metastatic pNETs. The mutation frequencies are expressed as the percentage of cases harboring ≥1 coding alteration. Each bubble represents one or more genes that share the same frequency pair and bubble size encodes the number of genes at that coordinate (legend, right). The red dashed diagonal marks parity between groups.

Figure 4. Canonical oncogenic pathway alterations and functional enrichment in hypermutated pNETs. A. Pathways impacted by the changes in mutational landscape in pNETs compared to normal pancreas tissues. Bar plots summarize the distribution of somatic alterations across major oncogenic signaling pathways. Pathways are ordered by the decreasing number of altered genes. For each pathway, the relative fraction of alterations among all pNET samples is

813 shown in the right panel. **B.** Gene-level mutation maps for canonical signaling pathways including
814 RTK-RAS, NOTCH, WNT and Hippo signaling. Columns represent individual tumors and rows
815 represent individual genes within each pathway. The red squares indicate the presence of at least
816 one somatic mutation in that gene in the corresponding tumor. Empty cells denote no detectable
817 coding alteration. Gene names in red mark core canonical drivers, whereas those in blue highlight
818 essential signaling or other potentially druggable components. **C.** Venn diagram depicting the
819 overlapping mutated gene numbers between non-metastatic and metastatic patient pNET samples.
820 Percentages representing the proportion of the combined gene set. **D.** Functional enrichment of top
821 twenty KEGG pathways in metastatic patient pNET samples as compared to non-metastatic
822 samples. **E.** Functional enrichment of top twenty hallmark gene sets in metastatic patient pNET
823 samples as compared to non-metastatic samples. Each dot corresponds to a significantly enriched
824 pathway or gene-ontology term. The x-axis denotes enrichment significance, the color scale
825 indicates fold-enrichment, and dot size reflects the number of genes from the input list contributing
826 to each term.
827
828 **Figure 5. Differential gene expressions in low-grade pNET patient samples. A.** Volcano plot
829 of differentially expressed genes in pNET patient samples compared to normal pancreas. The x-
830 axis shows log2 fold-changes and the y-axis shows -$\log_{10}$ adjusted *P* value. Red and blue points
831 indicate significantly upregulated and downregulated genes, respectively. The top -up and -
832 downregulated genes are labelled. **B.** Unsupervised hierarchical clustering heatmap of
833 differentially expressed genes (DEGs). Each column represents an individual tumor and each row
834 a gene. Relative expressions depicted in a color scale where red indicates higher expression and
835 blue indicates lower expression. The annotation bars below the heatmap indicate
836 clinical/pathologic features for each sample: Group, metastatic status, WHO grade (G1 and G2)
837 and tumor size (≤2 cm vs >2 cm). **C.** Horizontal bar plots showing the functional enrichment
838 analysis of DEG between non-metastatic and metastatic tumors. The top KEGG and Gene
839 Ontology (GO; biological process, cellular component and molecular function) enrichments are
840 ranked by significance. **D.** DEG associated functional enrichment of top twenty KEGG pathways
841 in metastatic patient pNET samples as compared to non-metastatic samples. **E.** DEG associated
842 functional of top twenty hallmark gene sets in metastatic patient pNET samples as compared to
843 non-metastatic samples. Each dot corresponds to a significantly enriched pathway or GO term.

844 The x-axis denotes enrichment significance, the color scale indicates fold-enrichment, and dot size
845 reflects the number of genes from the input list contributing to each term.

846 **Figure 6. Integration of mutational alterations and transcriptional changes derived from**
847 **same tumors highlights key genes and pathways in low-grade pNETs. A.** Venn diagram
848 showing the overlap between significantly mutated genes and differentially expressed genes
849 (DEGs) in low-grade pNETs. Number of genes are indicated in each segment. Mutational
850 frequency of overlapping genes in non-metastatic and metastatic pNET samples are shown in the
851 lower panel. **B-C.** Key pathways associated with overlapped genes. Upper panel indicates gene
852 mutation frequencies both in non-metastatic (right) and metastatic (left) pNET samples. Lower
853 heatmap indicates the count of DEGs in non-metastatic (pink) and metastatic (blue) pNET
854 samples. Columns represent samples and rows represent genes. **B.** Calcium signaling pathway. **C.**
855 WNT signaling pathway. **D.** Hallmark KRAS-signaling-DN gene set and association with
856 overlapped genes. Upper panel indicates gene mutation frequencies both in non-metastatic (right)
857 and metastatic (left) pNET samples. Lower heatmap indicates the count of DEGs in non-metastatic
858 (pink) and metastatic (blue) pNET samples. Columns represent samples and rows represent genes.
859 **E-G.** Gene set enrichment analysis (GSEA) of calcium signaling, WNT signaling and PI3K-AKT
860 signaling pathways. The enrichment plot shows normalized enrichment score (NES) for the KEGG
861 pathways in metastatic pNETs compared to non-metastatic tumors as a function of the ranked gene
862 list. **H.** Lollipop plot of ZNF273 (NM_021148) somatic mutations in non-metastatic primary
863 pNETs (n = 56). The linear schematic depicts the ZNF273 protein with the N-terminal KRAB_A-
864 Box domain and C-terminal zinc-finger region (zf-H2C2_2). Each lollipop represents a somatic
865 variant identified by whole-exome sequencing, plotted at its codon position. **I.** Corresponding
866 lollipop plot for metastatic primary pNETs (n = 19). Domain structure and scaling are identical to
867 panel H.

868 **Figure 7. Clinically actionable genetic alterations observed in low-grade pNETs with**
869 **metastatic status. A.** iPathwayGuide analysis (Advaita Corp. 2025) of gene expressions in
870 metastatic pNETs compared to non-metastatic pNETs predicted drugs that could have actionable
871 changes in low-grade pNETs that have metastasized in the patients. The prediction of upstream
872 drugs is based on the enrichment of differentially expressed genes (DEGs) from the experiment
873 and a network of interactions from the Advaita Knowledge Base (AKB v18.1). Bar diagram

874 indicates number of consistent DEGs. **B.** iPathwayGuide analysis of gene expressions in metastatic
875 pNETs compared to non-metastatic pNETs predicted drugs that may not have actionable changes
876 in low-grade pNETs have metastasized in the patients. Bar diagram indicates number of consistent
877 DEGs. **C-D.** The Gene2Drug software predicted multiple drugs against topmost overlapped genes
878 (after integration of genetic alteration and gene expression data) observed in the study having high
879 tumor mutational burden in metastatic pNETs. DOWN indicates inhibitory effect. **C.** Gene2Drug-
880 predicted drugs against ZNF273 alterations. **D.** Gene2Drug-predicted drugs against RYR1
881 alterations. BP, biological pathway; CC, cellular component; CGP, cancer-related drug
882 perturbation data; DB, database; ES, enrichment score; MF, molecular function; TFT,
883 Transcription-factor-target sets.

884
885
886
887
888
889
890
891
892
893
894
895
896
897
898
899
900
901
902

903 **Figure 1**

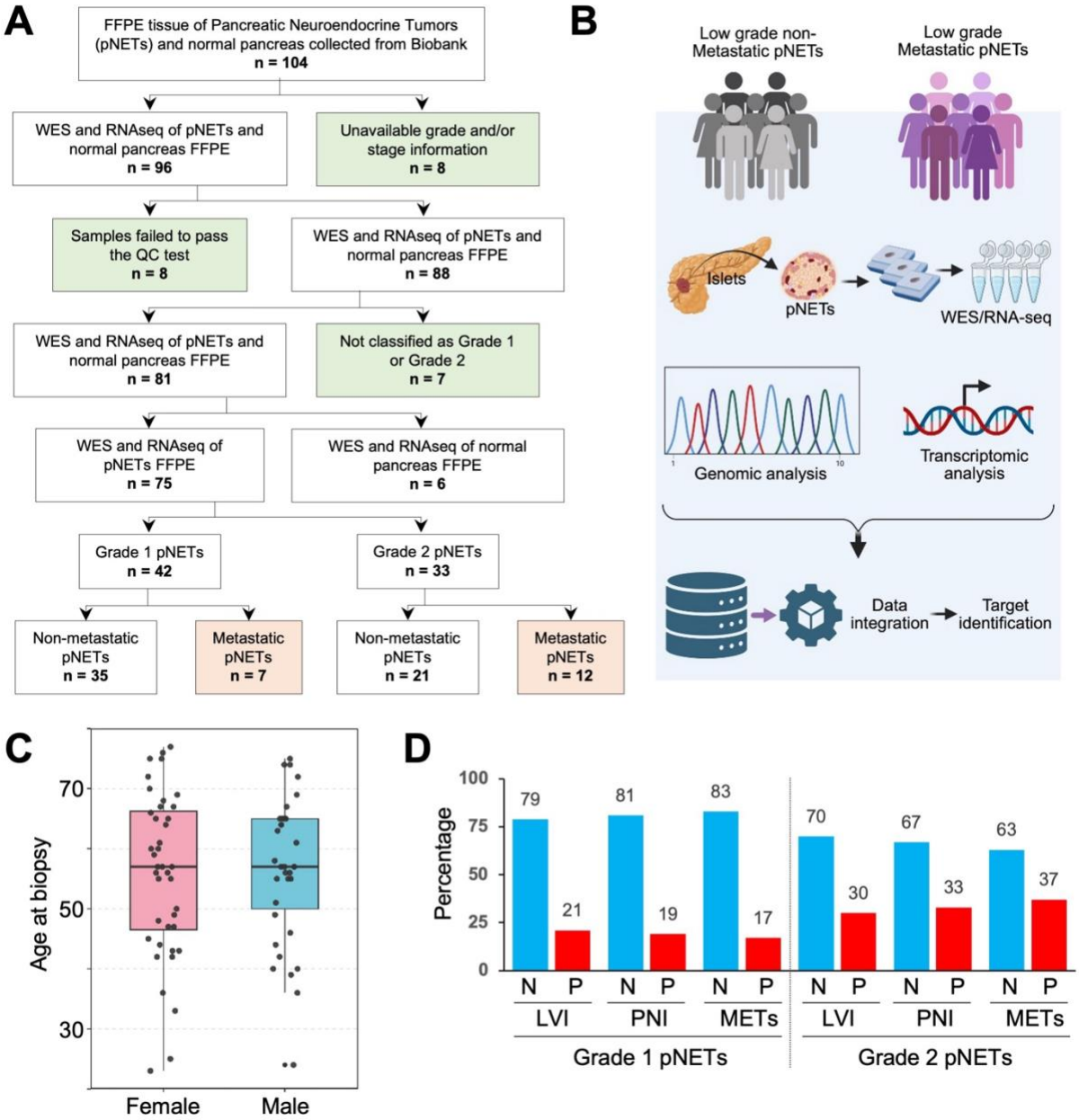

904

905

906

907

908

909

Figure 2

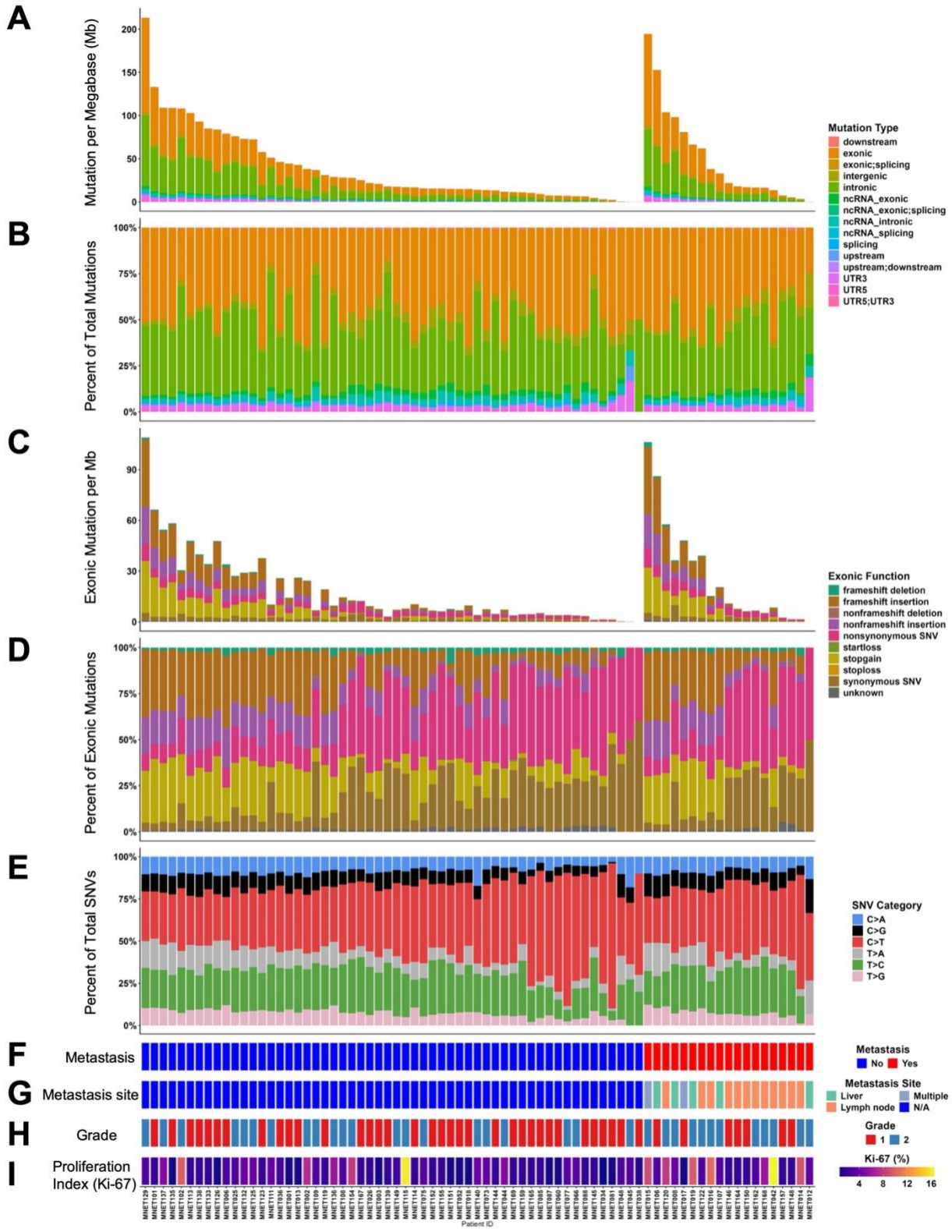
A
Mutation per Megabase (Mb)
B
Percent of Total Mutations
C
Exonic Mutation per Mb
D
Percent of Exonic Mutations
E
Percent of Total SNVs
F
Metastasis
G
Metastasis site
H
Grade
I
Proliferation Index (Ki-67)
Patient ID
Mutation Type
downstream
exonic
exonic;splicing
intergenic
intronic
ncRNA_exonic
ncRNA_exonic;splicing
ncRNA_intronic
ncRNA_splicing
splicing
upstream
upstream;downstream
UTR3
UTR5
UTR5;UTR3
Exonic Function
frameshift deletion
frameshift insertion
nonframeshift deletion
nonframeshift insertion
nonsynonymous SNV
startloss
stopgain
stoploss
synonymous SNV
unknown
SNV Category
C>A
C>G
C>T
T>A
T>C
T>G
Metastasis
No
Yes
Metastasis Site
Liver
Multiple
Lymph node
N/A
Grade
1
2
Ki-67 (%)
4
8
12
16

Figure 3

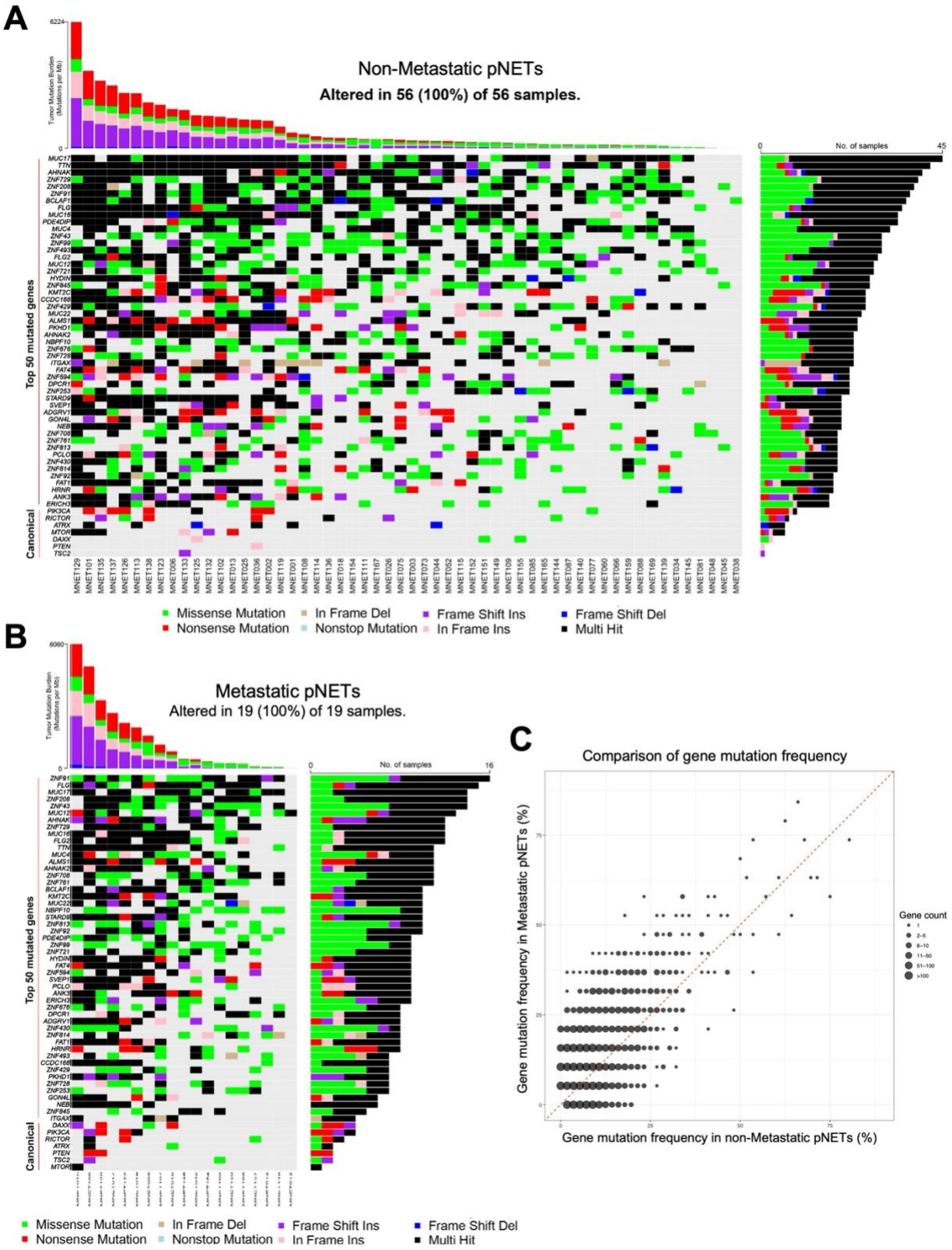
A
Non-Metastatic pNETs
Altered in 56 (100%) of 56 samples.
Tumor Mutation Burden (Mutations per Mb)
No. of samples
Top 50 mutated genes
Canonical
Missense Mutation
Nonsense Mutation
In Frame Del
Nonstop Mutation
Frame Shift Ins
In Frame Ins
Frame Shift Del
Multi Hit
B
Metastatic pNETs
Altered in 19 (100%) of 19 samples.
C
Comparison of gene mutation frequency
Gene mutation frequency in Metastatic pNETs (%)
Gene mutation frequency in non-Metastatic pNETs (%)
Gene count

Figure 4

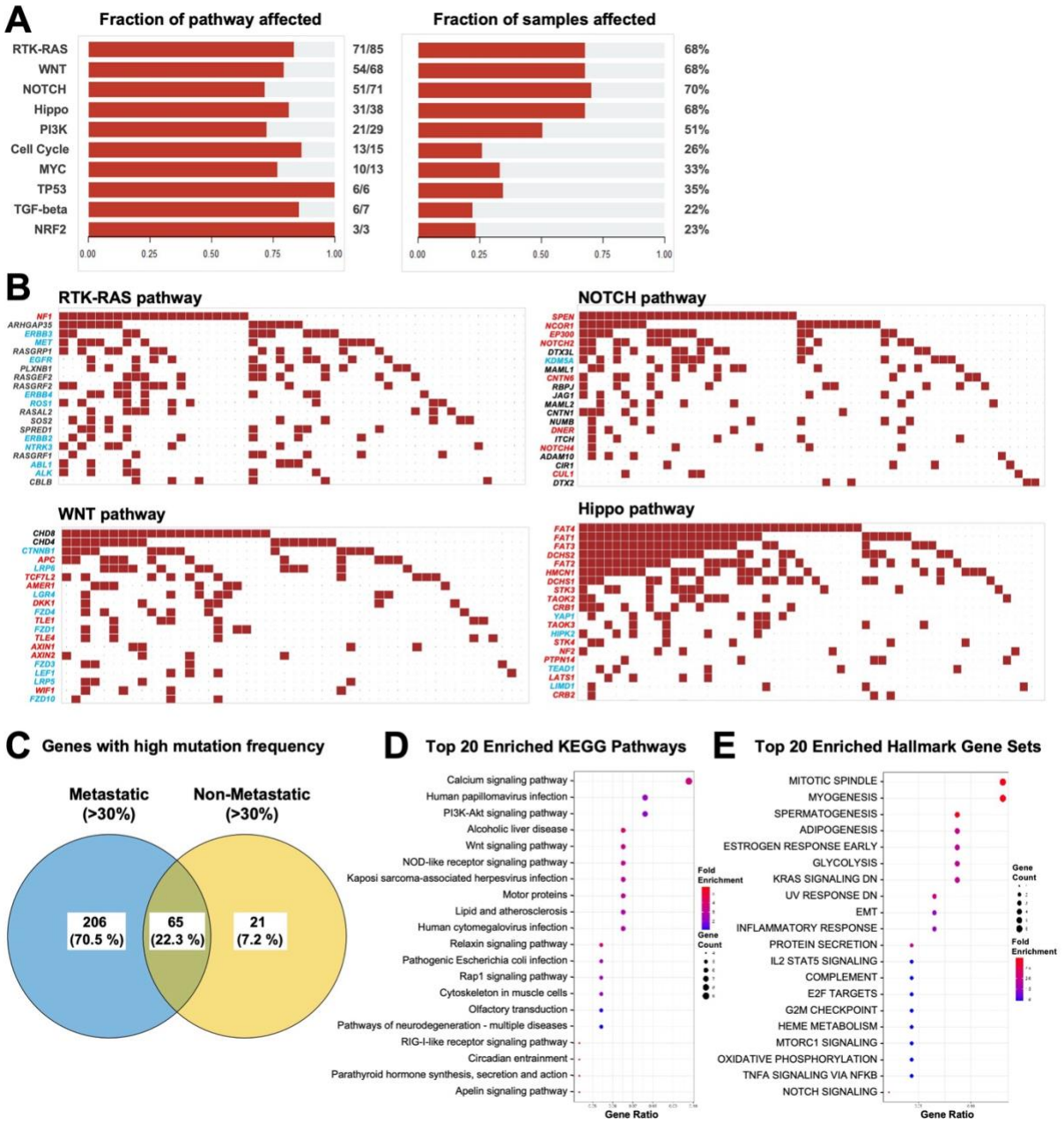
A
Fraction of pathway affected
Fraction of samples affected
RTK-RAS 71/85 68%
WNT 54/68 68%
NOTCH 51/71 70%
Hippo 31/38 68%
PI3K 21/29 51%
Cell Cycle 13/15 26%
MYC 10/13 33%
TP53 6/6 35%
TGF-beta 6/7 22%
NRF2 3/3 23%
B
RTK-RAS pathway
NOTCH pathway
WNT pathway
Hippo pathway
C Genes with high mutation frequency
Metastatic (>30%)
Non-Metastatic (>30%)
206 (70.5 %)
65 (22.3 %)
21 (7.2 %)
D Top 20 Enriched KEGG Pathways
Calcium signaling pathway
Human papillomavirus infection
PI3K-Akt signaling pathway
Alcoholic liver disease
Wnt signaling pathway
NOD-like receptor signaling pathway
Kaposi sarcoma-associated herpesvirus infection
Motor proteins
Lipid and atherosclerosis
Human cytomegalovirus infection
Relaxin signaling pathway
Pathogenic Escherichia coli infection
Rap1 signaling pathway
Cytoskeleton in muscle cells
Olfactory transduction
Pathways of neurodegeneration - multiple diseases
RIG-I-like receptor signaling pathway
Circadian entrainment
Parathyroid hormone synthesis, secretion and action
Apelin signaling pathway
Gene Ratio
Fold Enrichment
Gene Count
E Top 20 Enriched Hallmark Gene Sets
MITOTIC SPINDLE
MYOGENESIS
SPERMATOGENESIS
ADIPOGENESIS
ESTROGEN RESPONSE EARLY
GLYCOLYSIS
KRAS SIGNALING DN
UV RESPONSE DN
EMT
INFLAMMATORY RESPONSE
PROTEIN SECRETION
IL2 STAT5 SIGNALING
COMPLEMENT
E2F TARGETS
G2M CHECKPOINT
HEME METABOLISM
MTORC1 SIGNALING
OXIDATIVE PHOSPHORYLATION
TNFA SIGNALING VIA NFKB
NOTCH SIGNALING
Gene Ratio
Gene Count
Fold Enrichment

Figure 5

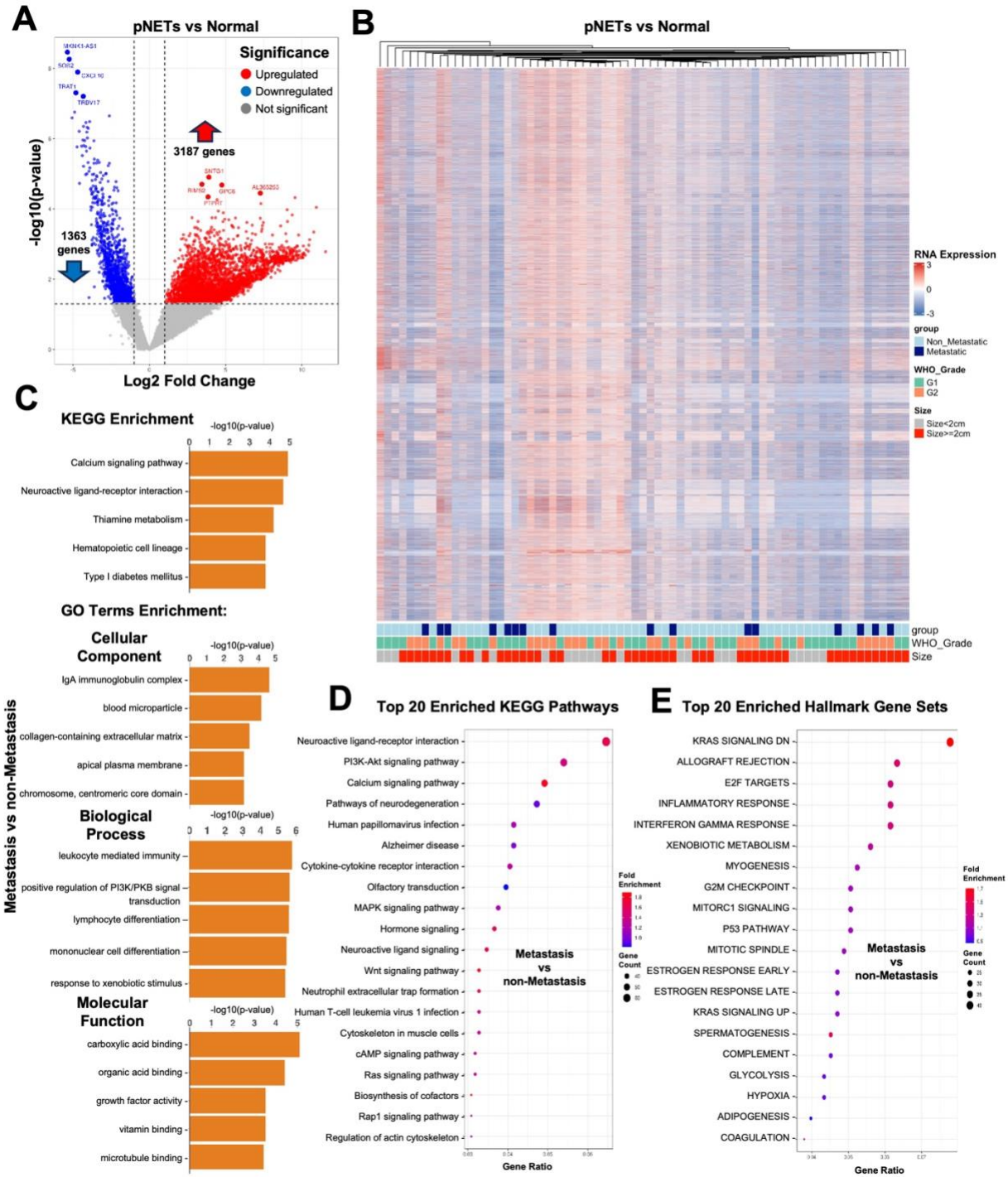
A
pNETs vs Normal
Significance
Upregulated
Downregulated
Not significant
3187 genes
1363 genes
-log10(p-value)
Log2 Fold Change
B
pNETs vs Normal
RNA Expression
group
Non_Metastatic
Metastatic
WHO_Grade
G1
G2
Size
Size<2cm
Size>=2cm
C
KEGG Enrichment
-log10(p-value)
Calcium signaling pathway
Neuroactive ligand-receptor interaction
Thiamine metabolism
Hematopoietic cell lineage
Type I diabetes mellitus
GO Terms Enrichment:
Cellular Component
IgA immunoglobulin complex
blood microparticle
collagen-containing extracellular matrix
apical plasma membrane
chromosome, centromeric core domain
Biological Process
leukocyte mediated immunity
positive regulation of PI3K/PKB signal transduction
lymphocyte differentiation
mononuclear cell differentiation
response to xenobiotic stimulus
Molecular Function
carboxylic acid binding
organic acid binding
growth factor activity
vitamin binding
microtubule binding
Metastasis vs non-Metastasis
D
Top 20 Enriched KEGG Pathways
Neuroactive ligand-receptor interaction
PI3K-Akt signaling pathway
Calcium signaling pathway
Pathways of neurodegeneration
Human papillomavirus infection
Alzheimer disease
Cytokine-cytokine receptor interaction
Olfactory transduction
MAPK signaling pathway
Hormone signaling
Neuroactive ligand signaling
Wnt signaling pathway
Neutrophil extracellular trap formation
Human T-cell leukemia virus 1 infection
Cytoskeleton in muscle cells
cAMP signaling pathway
Ras signaling pathway
Biosynthesis of cofactors
Rap1 signaling pathway
Regulation of actin cytoskeleton
Metastasis vs non-Metastasis
Fold Enrichment
Gene Count
Gene Ratio
E
Top 20 Enriched Hallmark Gene Sets
KRAS SIGNALING DN
ALLOGRAFT REJECTION
E2F TARGETS
INFLAMMATORY RESPONSE
INTERFERON GAMMA RESPONSE
XENOBIOTIC METABOLISM
MYOGENESIS
G2M CHECKPOINT
MITORC1 SIGNALING
P53 PATHWAY
MITOTIC SPINDLE
ESTROGEN RESPONSE EARLY
ESTROGEN RESPONSE LATE
KRAS SIGNALING UP
SPERMATOGENESIS
COMPLEMENT
GLYCOLYSIS
HYPOXIA
ADIPOGENESIS
COAGULATION
Metastasis vs non-Metastasis
Fold Enrichment
Gene Count
Gene Ratio

Figure 6

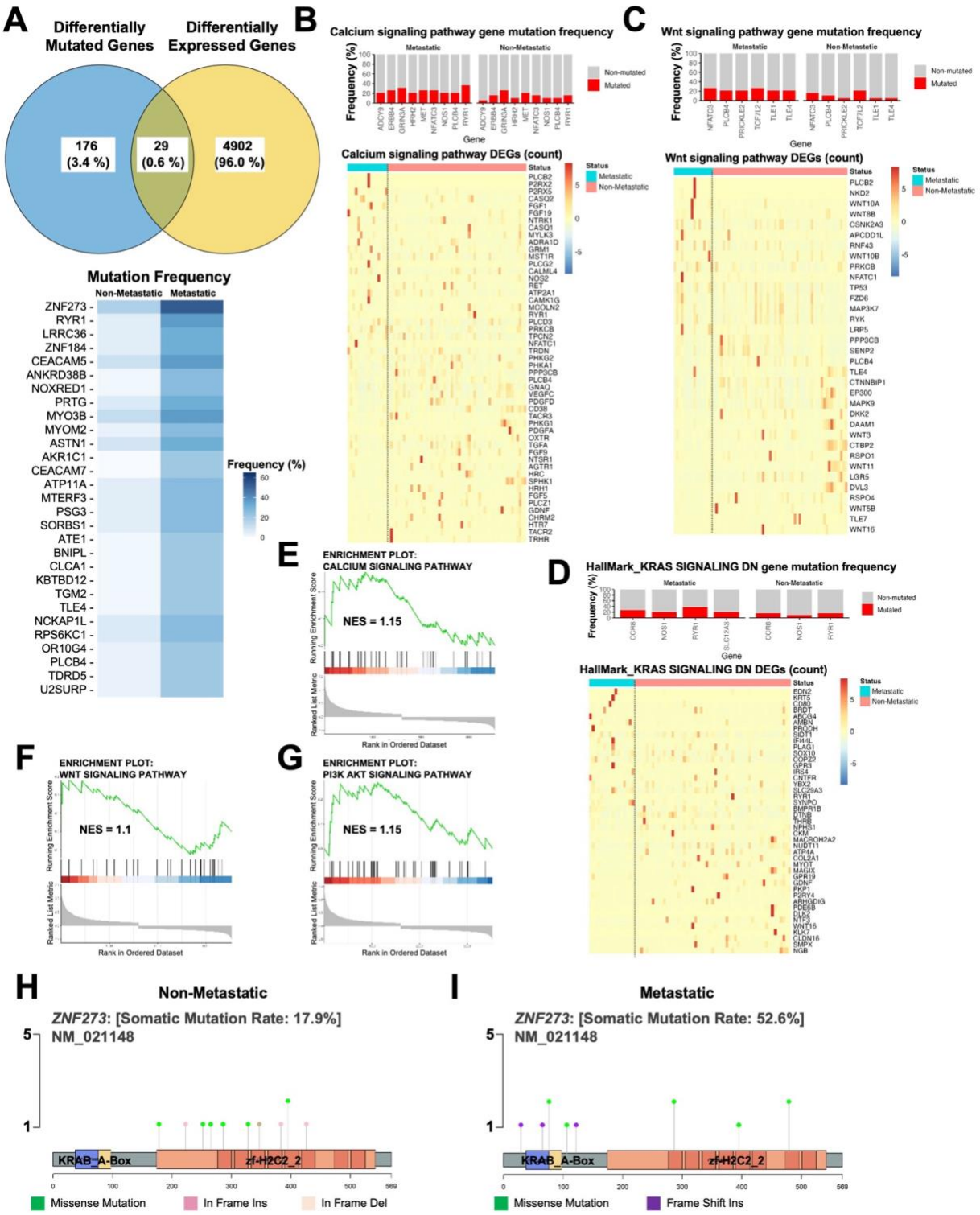
A
Differentially Mutated Genes
Differentially Expressed Genes
176 (3.4 %)
29 (0.6 %)
4902 (96.0 %)
Mutation Frequency
Non-Metastatic
Metastatic
Frequency (%)
B
Calcium signaling pathway gene mutation frequency
Calcium signaling pathway DEGs (count)
C
Wnt signaling pathway gene mutation frequency
Wnt signaling pathway DEGs (count)
D
HallMark_KRAS SIGNALING DN gene mutation frequency
HallMark_KRAS SIGNALING DN DEGs (count)
E
ENRICHMENT PLOT: CALCIUM SIGNALING PATHWAY
NES = 1.15
F
ENRICHMENT PLOT: WNT SIGNALING PATHWAY
NES = 1.1
G
ENRICHMENT PLOT: PI3K AKT SIGNALING PATHWAY
NES = 1.15
H
Non-Metastatic
ZNF273: [Somatic Mutation Rate: 17.9%]
NM_021148
KRAB
A-Box
zf-H2C2_2
Missense Mutation
In Frame Ins
In Frame Del
I
Metastatic
ZNF273: [Somatic Mutation Rate: 52.6%]
NM_021148
KRAB
A-Box
zf-H2C2_2
Missense Mutation
Frame Shift Ins

925 **Figure 7**

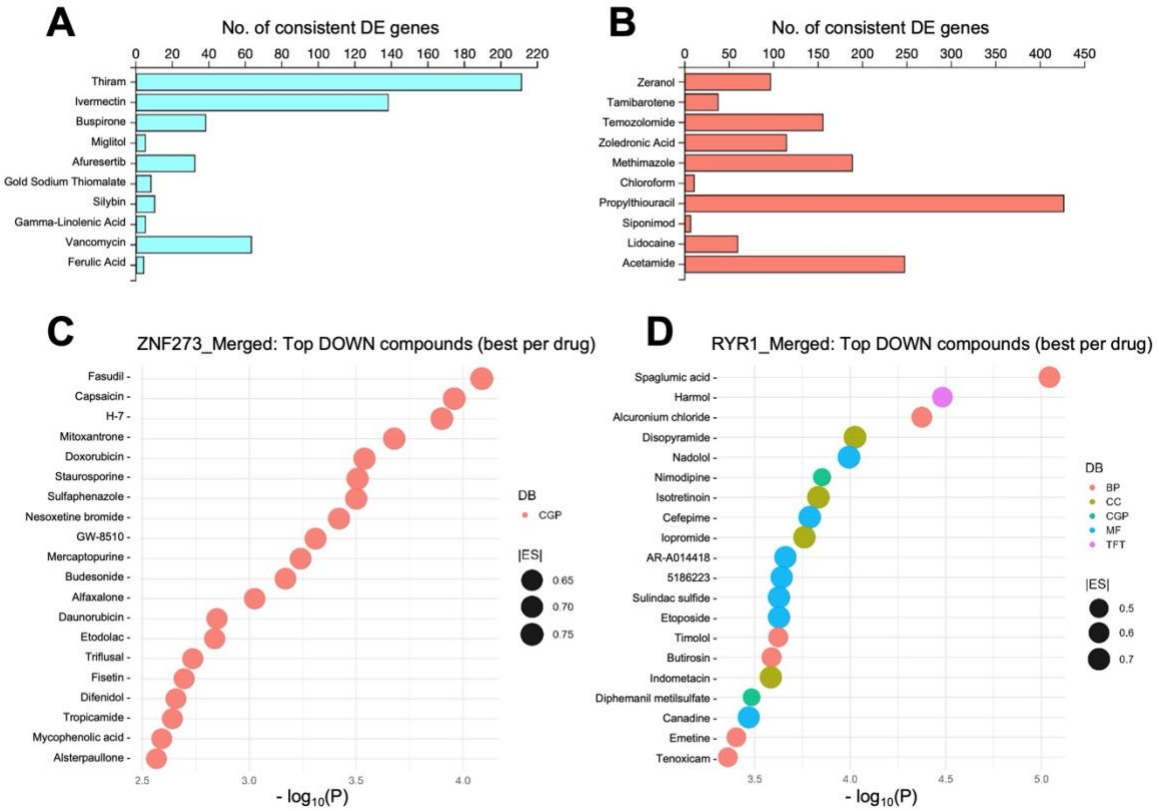

926

927

928 **Table 1**: **Clinical and Demographic Characteristics of Low-Grade pNET Patients.**

929

Parameter	Sex	Frequency	Percentage (%)
Sex	Male	34	45.33
	Female	41	54.67
	Total	75	100
Median age (range)	Male	57 (51)	-
	Female	57 (58)	-
	Total	57 (58)	-
Average age	Male	57.11	-
	Female	54.76	-
	Total	55.83	-
Tumor grade 1	Male	19	45.24
	Female	23	54.76
	Total	42	100
Tumor grade 2	Male	15	45.45
	Female	18	54.54
	Total	33	100
T-stage	Male		
	Stage 1	8	-
	Stage 2	16	-
	Stage 3	9	-
	Stage 4	1	-
	Female		
	Stage 1	14	-
	Stage 2	15	-
	Stage 3	9	-
	Stage 4	2	-
	Undetermined	1	-
N-stage	Male		
	Stage 0	21	-
	Stage 1	11	-
	pNx	2	-
	Female		
	Stage 0	28	-
	Stage 1	10	-
	pNx	2	-
	N/A	1	-
LN-status	Male		
	Positive	11	-
	Negative	21	-
	N/A	2	-

	Female		
	Positive	11	-
	Negative	27	-
	N/A	3	-
Metastasis	Male		
	Yes	10	-
	No	22	-
	N/A	1	-
	Undetermined	1	-
	Female		
	Yes	9	-
	No	31	-
	N/A	1	-

Abbreviations: T-stage, tumor stage; N-stage, neural stage; LN, lymph node; N/A, not applicable; pNx, undetermined peri neural invasion.

947 **References**

948

949 1 Oronsky, B., Ma, P. C., Morgensztern, D. & Carter, C. A. Nothing But NET: A Review of
950 Neuroendocrine Tumors and Carcinomas. *Neoplasia* **19**, 991-1002,
951 doi:10.1016/j.neo.2017.09.002 (2017).
952 2 Mpilla, G. B., Philip, P. A., El-Rayes, B. & Azmi, A. S. Pancreatic neuroendocrine tumors:
953 Therapeutic challenges and research limitations. *World J Gastroenterol* **26**, 4036-4054,
954 doi:10.3748/wjg.v26.i28.4036 (2020).
955 3 Das, S. & Dasari, A. Epidemiology, Incidence, and Prevalence of Neuroendocrine Neoplasms: Are
956 There Global Differences? *Curr Oncol Rep* **23**, 43, doi:10.1007/s11912-021-01029-7 (2021).
957 4 Dasari, A. *et al.* Trends in the Incidence, Prevalence, and Survival Outcomes in Patients With
958 Neuroendocrine Tumors in the United States. *JAMA Oncol* **3**, 1335-1342,
959 doi:10.1001/jamaoncol.2017.0589 (2017).
960 5 Geurts, J. L. Inherited syndromes involving pancreatic neuroendocrine tumors. *J Gastrointest*
961 *Oncol* **11**, 559-566, doi:10.21037/jgo.2020.03.09 (2020).
962 6 Stevenson, M., Lines, K. E. & Thakker, R. V. Molecular Genetic Studies of Pancreatic
963 Neuroendocrine Tumors: New Therapeutic Approaches. *Endocrinol Metab Clin North Am* **47**,
964 525-548, doi:10.1016/j.ecl.2018.04.007 (2018).
965 7 Jiao, Y. *et al.* DAXX/ATRX, MEN1, and mTOR pathway genes are frequently altered in pancreatic
966 neuroendocrine tumors. *Science* **331**, 1199-1203, doi:10.1126/science.1200609 (2011).
967 8 Missiaglia, E. *et al.* Pancreatic endocrine tumors: expression profiling evidences a role for AKT-
968 mTOR pathway. *J Clin Oncol* **28**, 245-255, doi:10.1200/JCO.2008.21.5988 (2010).
969 9 Scarpa, A. *et al.* Whole-genome landscape of pancreatic neuroendocrine tumours. *Nature* **543**,
970 65-71, doi:10.1038/nature21063 (2017).
971 10 Zhang, J. *et al.* Current understanding of the molecular biology of pancreatic neuroendocrine
972 tumors. *J Natl Cancer Inst* **105**, 1005-1017, doi:10.1093/jnci/djt135 (2013).
973 11 Maxwell, J. E., Sherman, S. K. & Howe, J. R. Translational Diagnostics and Therapeutics in
974 Pancreatic Neuroendocrine Tumors. *Clin Cancer Res* **22**, 5022-5029, doi:10.1158/1078-
975 0432.CCR-16-0435 (2016).
976 12 Beyens, M., Vandamme, T., Peeters, M., Van Camp, G. & Op de Beeck, K. Resistance to targeted
977 treatment of gastroenteropancreatic neuroendocrine tumors. *Endocr Relat Cancer* **26**, R109-
978 R130, doi:10.1530/ERC-18-0420 (2019).

979 13 Vandamme, T. *et al.* Hotspot DAXX, PTCH2 and CYFIP2 mutations in pancreatic neuroendocrine
980 neoplasms. *Endocr Relat Cancer* **26**, 1-12, doi:10.1530/ERC-18-0120 (2019).
981 14 Yao, J. C. *et al.* Everolimus for advanced pancreatic neuroendocrine tumors. *N Engl J Med* **364**,
982 514-523, doi:10.1056/NEJMoa1009290 (2011).
983 15 Raymond, E. *et al.* Sunitinib malate for the treatment of pancreatic neuroendocrine tumors. *N*
984 *Engl J Med* **364**, 501-513, doi:10.1056/NEJMoa1003825 (2011).
985 16 Faes, S., Demartines, N. & Dormond, O. Resistance to mTORC1 Inhibitors in Cancer Therapy:
986 From Kinase Mutations to Intratumoral Heterogeneity of Kinase Activity. *Oxid Med Cell Longev*
987 **2017**, 1726078, doi:10.1155/2017/1726078 (2017).
988 17 Avanthay, S. *et al.* Molecular Subtypes of Pancreatic Neuroendocrine Tumors Mutated in
989 MEN1/DAXX/ATRX Explain Biological Variability. *Endocr Pathol* **36**, 44, doi:10.1007/s12022-025-
990 09889-6 (2025).
991 18 Chan, C. S. *et al.* ATRX, DAXX or MEN1 mutant pancreatic neuroendocrine tumors are a distinct
992 alpha-cell signature subgroup. *Nat Commun* **9**, 4158, doi:10.1038/s41467-018-06498-2 (2018).
993 19 Yasunaga, Y., Tanaka, M., Arita, J., Hasegawa, K. & Ushiku, T. Loss of ATRX and DAXX in
994 pancreatic neuroendocrine tumors: Association with recurrence risk, cellular phenotype, and
995 heterogeneity. *Hum Pathol* **150**, 51-57, doi:10.1016/j.humpath.2024.06.015 (2024).
996 20 Huang, S., Soto, A. M. & Sonnenschein, C. The end of the genetic paradigm of cancer. *PLoS Biol*
997 **23**, e3003052, doi:10.1371/journal.pbio.3003052 (2025).
998 21 Sadowski, S. M., Pieterman, C. R. C., Perrier, N. D., Triponez, F. & Valk, G. D. Prognostic factors
999 for the outcome of nonfunctioning pancreatic neuroendocrine tumors in MEN1: a systematic
1000 review of literature. *Endocr Relat Cancer* **27**, R145-R161, doi:10.1530/ERC-19-0372 (2020).
1001 22 Galasso, L. *et al.* Decoding Pancreatic Neuroendocrine Tumors: Molecular Profiles, Biomarkers,
1002 and Pathways to Personalized Therapy. *Int J Mol Sci* **26**, doi:10.3390/ijms26167814 (2025).
1003 23 Briest, F. & Grabowski, P. PI3K-AKT-mTOR-signaling and beyond: the complex network in
1004 gastroenteropancreatic neuroendocrine neoplasms. *Theranostics* **4**, 336-365,
1005 doi:10.7150/thno.7851 (2014).
1006 24 Saleh, Z. *et al.* Pancreatic Neuroendocrine Tumors: Signaling Pathways and Epigenetic
1007 Regulation. *Int J Mol Sci* **25**, doi:10.3390/ijms25021331 (2024).
1008 25 Ahsan, S. & Draghici, S. Identifying Significantly Impacted Pathways and Putative Mechanisms
1009 with iPathwayGuide. *Curr Protoc Bioinformatics* **57**, 7 15 11-17 15 30, doi:10.1002/cpbi.24
1010 (2017).

1011 26 Napolitano, F. *et al.* gene2drug: a computational tool for pathway-based rational drug
1012 repositioning. *Bioinformatics* **34**, 1498-1505, doi:10.1093/bioinformatics/btx800 (2018).
1013 27 Zhang, L. *et al.* Ryanodine receptor 1-mediated Ca(2+) signaling and mitochondrial
1014 reprogramming modulate uterine serous cancer malignant phenotypes. *J Exp Clin Cancer Res* **41**,
1015 242, doi:10.1186/s13046-022-02419-w (2022).
1016 28 Peculis, R. *et al.* Whole exome sequencing reveals novel risk genes of pituitary neuroendocrine
1017 tumors. *PLoS One* **17**, e0265306, doi:10.1371/journal.pone.0265306 (2022).
1018 29 Pertea, M. *et al.* StringTie enables improved reconstruction of a transcriptome from RNA-seq
1019 reads. *Nat Biotechnol* **33**, 290-295, doi:10.1038/nbt.3122 (2015).
1020 30 Uddin, M. H. *et al.* Aberrant transcription factors in the cancers of the pancreas. *Semin Cancer*
1021 *Biol* **86**, 28-45, doi:10.1016/j.semcancer.2022.08.011 (2022).
1022 31 Andersen, K. O., Detlefsen, S., Brusgaard, K. & Christesen, H. T. Well-differentiated G1 and G2
1023 pancreatic neuroendocrine tumors: a meta-analysis of published expanded DNA sequencing
1024 data. *Front Endocrinol (Lausanne)* **15**, 1351624, doi:10.3389/fendo.2024.1351624 (2024).
1025 32 Xu, J. *et al.* Recent research hotspots in sequencing and the pancreatic neuroendocrine tumor
1026 microenvironment. *Cancer Biol Med* **20**, 721-727, doi:10.20892/j.issn.2095-3941.2023.0284
1027 (2023).
1028 33 Pipinikas, C. P., Berner, A. M., Sposito, T. & Thirlwell, C. The evolving (epi)genetic landscape of
1029 pancreatic neuroendocrine tumours. *Endocr Relat Cancer* **26**, R519-R544, doi:10.1530/ERC-19-
1030 0175 (2019).
1031 34 Scott, A. T. *et al.* Gene Expression Signatures Identify Novel Therapeutics for Metastatic
1032 Pancreatic Neuroendocrine Tumors. *Clin Cancer Res* **26**, 2011-2021, doi:10.1158/1078-
1033 0432.CCR-19-2884 (2020).
1034 35 Bettaieb, L. *et al.* Ca(2+) Signaling and Its Potential Targeting in Pancreatic Ductal Carcinoma.
1035 *Cancers (Basel)* **13**, doi:10.3390/cancers13123085 (2021).
1036 36 Stopa, K. B. *et al.* Driver Mutations of Pancreatic Cancer Affect Ca(2+) Signaling and ATP
1037 Production. *Function (Oxf)* **4**, zqad035, doi:10.1093/function/zqad035 (2023).
1038 37 Weissenrieder, J. S. *et al.* Mitochondrial Ca(2+) controls pancreatic cancer growth and
1039 metastasis by regulating epithelial cell plasticity. *bioRxiv*, doi:10.1101/2024.08.08.607195
1040 (2024).
1041 38 Kim, J. T. *et al.* Neurotensin, a novel target of Wnt/beta-catenin pathway, promotes growth of
1042 neuroendocrine tumor cells. *Int J Cancer* **136**, 1475-1481, doi:10.1002/ijc.29123 (2015).

1043 39 Weiss, V. *et al.* Immunohistochemical analysis of the Wnt/beta-catenin signaling pathway in
1044 pancreatic neuroendocrine neoplasms. *World J Gastrointest Oncol* **8**, 615-622,
1045 doi:10.4251/wjgo.v8.i8.615 (2016).
1046 40 Mafficini, A. & Scarpa, A. Genomic landscape of pancreatic neuroendocrine tumours: the
1047 International Cancer Genome Consortium. *J Endocrinol* **236**, R161-R167, doi:10.1530/JOE-17-
1048 0560 (2018).
1049 41 Maharjan, C. K. *et al.* Pancreatic Neuroendocrine Tumors: Molecular Mechanisms and
1050 Therapeutic Targets. *Cancers (Basel)* **13**, doi:10.3390/cancers13205117 (2021).
1051 42 Munro, D., Ghersi, D. & Singh, M. Two critical positions in zinc finger domains are heavily
1052 mutated in three human cancer types. *PLoS Comput Biol* **14**, e1006290,
1053 doi:10.1371/journal.pcbi.1006290 (2018).
1054 43 Machnik, M. *et al.* The expression signature of cancer-associated KRAB-ZNF factors identified in
1055 TCGA pan-cancer transcriptomic data. *Mol Oncol* **13**, 701-724, doi:10.1002/1878-0261.12407
1056 (2019).
1057 44 Sobocinska, J., Molenda, S., Machnik, M. & Oleksiewicz, U. KRAB-ZFP Transcriptional Regulators
1058 Acting as Oncogenes and Tumor Suppressors: An Overview. *Int J Mol Sci* **22**,
1059 doi:10.3390/ijms22042212 (2021).
1060 45 Raj, N. *et al.* Real-Time Genomic Characterization of Metastatic Pancreatic Neuroendocrine
1061 Tumors Has Prognostic Implications and Identifies Potential Germline Actionability. *JCO Precis*
1062 *Oncol* **2018**, doi:10.1200/PO.17.00267 (2018).

1063